Mateus, A. *et al.* 2005. Variscan overthrusting, fluid flow and the genesis of magnetite ore-bodies at Azenhas area (Pedrógão, Ossa-Morena Zone, SE Portugal). *Boletín Geológico y Minero,* 116 (1): 3-22
ISSN: 0366-0176

Variscan overthrusting, fluid flow and the genesis of magnetite ore-bodies at Azenhas area (Pedrógão, Ossa-Morena Zone, SE Portugal)

A. Mateus[(1)], A. Araújo[(2)]*, M.A. Gonçalves[(3)] y J. Matos[(4)]

(1) Dept. Geologia and CREMINER, Fac. Ciências, Univ. Lisboa. Edifício C6, Piso 4, Campo Grande. 1749-016 Lisboa. Portugal.
E-mail: amateus@fc.ul.pt

(2) Dept. Geociências and Centro de Geofísica de Évora, Univ. Évora. Apartado 94. 7002-554 Évora. Portugal.
* Corresponding author E-mail: aaraujo@uevora.pt

(3) Dept. Geologia and CREMINER, Fac. Ciências, Univ. Lisboa. Edifício C6, Piso 4, Campo Grande. 1749-016 Lisboa. Portugal.
E-mail: mario.goncalves@fc.ul.pt

(4) Dept. Geociências, Univ. Évora. Apartado 94. 7002-554 Évora. Portugal.

ABSTRACT

In the Azenhas area (SE Portugal), an important segment of a regional WNW-ESE Variscan thrust can be observed. The hanging wall felsic metavolcanics carried from ENE are evolved rhyolite tuffs. The underlying sequence is mainly composed of variably metasomatised allochthonous amphibolites that are believed to represent an ophiolite slice tectonically overlying the autochthonous Moura-Ficalho Complex. Within this latter sequence, numerous WNW-ESE thrusts with prevailing displacement towards W-SW cut prior sub-parallel structures with northwards thrust shear. According to the observed crosscutting relationships and to the available petrographic data, the metasomatism experienced by the lower amphibolite sequence took place mainly before the emplacement of the upper slices of amphibolites, preceding therefore the installation of the felsic metatuffs. Magnetite ore-bodies are found within strongly metasomatised amphibolites immediately below the major WNW-ESE thrust zone or its subsidiary thrust structures. Their genesis is envisaged as a result of a complex chemical reaction path that involves the ascent of aqueous oxidising fluids under a reverse temperature gradient generated during the tectonic emplacement of amphibolites. In order to test the geological plausibility of the thermal evolution and the time span needed for ore genesis a one-dimensional numerical model was developed. This model enables the tracing of vertical thermal profiles at different times and accounts for the thrust emplacement history, incorporating variable erosion rates of the rock sequence. The results obtained show that an inverted thermal gradient in the thrusted sequence is kept for over 1 Ma and a regular temperature increase (from 400ºC to 500ºC) is observed in the underlying rocks lasting for 4.5 to 5.5 Ma.

Key words: inverted thermal gradients, Magnetite ores, over-thrust sequence, oxidising ore fluids, thermal driven fluid flow

Cabalgamiento Varisco, flujo de fluidos y génesis de yacimientos de magnetita en el área de Azenhas (Pedrógão, Zona Ossa-Morena, SE de Portugal)

RESUMEN

En la zona de Azenhas (SE de Portugal) aflora un importante segmento de un cabalgamiento regional varisco de dirección ONO-ESE. Las metavulcanitas félsicas del bloque superior, provenientes del ENE son tobas riolíticas evolucionadas. La secuencia infrayacente está compuesta fundamentalmente por anfibolitas alóctonas metasomatizadas en distinto grado, que representan una escama ofiolítica que se sitúa sobre el complejo autóctono de Moura-Ficalho. Dentro de esta última secuencia aparecen numerosos cabalgamientos de dirección ONO-ESE con desplazamiento preferente hacia el O-SO que cortan a estructuras previas subparalelas con cizalla inversa hacia el norte. De acuerdo con las relaciones de corte observadas y los datos petrográficos el metasomatismo sufrido por la secuencia anfibolítica inferior tuvo lugar principalmente antes del emplazamiento de las escamas superiores de anfibolitas, precediendo por tanto al emplazamiento de las metatobas félsicas. Aparecen lentejones de magnetita dentro de las anfibolitas fuertemente metasomatizadas inmediatamente debajo de la zona de cabalgamientos principal de dirección ONO-ESE o bien en estructuras cabalgantes subordinadas. Su génesis se interpretata como el resultado de reacciones químicas complejas que involucran el ascenso de fluidos acuosos oxidantes bajo un gradiente de temperatura inverso generado durante el emplazamiento tectónico de las anfibolitas. Se discute también la evolución térmica y el tiempo requerido para la formación de las menas, utilizando los resultados de un modelo numérico unidimensional que permite el trazado de perfiles térmicos verticales en diferentes momentos; el modelo incluye la historia de emplazamiento de los cabalgamientos e incorpora las tasas de erosión variable resultantes de la serie.

Palabras clave: fluidos mineralizantes oxidantes, flujo de fluidos controlado por temperaturas, gradientes geotérmicos invertidos, Menas de magnetita, secuencia de cabalgamientos

Introduction

The Ossa-Morena Zone (OMZ) is the most intriguing geotectonic unit of the Iberian Variscides whose singularities are still subject to intense debate (for a general review on the stratigraphy, structure, magmatism and metamorphism of the OMZ, see Quesada *et al*., 1990a, b; Liñán and Quesada, 1990; Robardet and Gutiérrez Marco, 1990; Apalategui *et al*., 1990; Sánchez Carretero *et al*., 1990; Quesada and Munhá, 1990; Quesada *et al*., 1994; Fonseca *et al*., 1999 and Eguiluz *et al*., 2000). Multiple sub-horizontal thrusting, often associated with kilometric recumbent folds, characterises the Palaeozoic tectonic evolution of the OMZ south-central domain. This has favoured the development of particular geological frameworks characterised by conspicuous over-thrust sequences. Whenever thermally contrasting, these sequences can expectably sustain inverted thermal gradients for enough time to trigger hydrothermal flows with metallogenic significance, whose potential still remains to be explored. Regional, WNW-ESE shear zones with prevailing sinistral kinematics subsequently affect the thrust belt.

A relatively well-exposed over-thrust sequence can be observed in the Azenhas area (Pedrógão, Serpa, SE Portugal), where some magnetite ore-bodies also occur. Former metallogenic models for these ore-bodies are reported in Silva (1945), Neiva (1952), Carvalho (1971) and Carvalho *et al*. (1971). These models considered ore genesis either as a skarn type product or a strabound-metamorphosed mineralisation related to volcanic activity. In this paper we propose and discuss an alternative model, in which the ore genesis is due to the rising of oxidising fluids along inverted thermal gradients induced by thrusting. In order to evaluate the geological record of the processes associated with fluid migration during the emplacement of the observed over-thrust sequence, a summary of the available field, petrographic and geochemical data (including mineral chemistry) is reported. We will also discuss the thermal evolution and the time span needed for ore genesis using the results of a one-dimensional numerical model that enables the tracing of thermal profiles at different times. This model accounts for the thrust emplacement history, as suggested by field data, and incorporates the resulting variable erosion rates of the overlying rock sequence.

Sampling and analytical procedures

Both a detailed geological mapping and sampling program was carried out in the Azenhas area in order to characterise the geochemical processes and the main mineralogical and textural transformations displayed by the outcropping rocks. Whole-rock chemical analysis were performed at Activation Laboratories Ltd (Canada) using the research grade package for 69 elements analysed by ICP, INAA, ICP/MS and XRF; estimated errors are usually less than 2% and 5-10% for major and trace elements, respectively. Mineral chemical compositions were analysed using a three-channel JEOL-JCXA 733 electron microprobe routinely operating with an accelerating voltage of 15 kV and beam currents of 25 and 15 nA for silicates and carbonates, respectively; oxides were analysed with a beam current of 25 nA and an accelerating voltage of 18 kV. Metallic (Cr), natural and synthetic mineral standards were used. Analytical quality was monitored by analysing those same standards before, during and after each work period; the estimated error is less than 2% for all the analysed elements.

Geological setting of the Azenhas area

A very schematic geological mapping of the region close to the Azenhas area is shown in Fig. 1. It reveals the presence of two main lithostratigraphic units separated by a major thrust zone and intruded by a late granite body, the Pedrógão pluton with a K-Ar radiometric age of 308±4 Ma (Carvalho, 1971). These units are partially covered by Cenozoic detrital sediments (mainly alluvial deposits of the Guadiana River). The upper unit, known as the Azenha da Rabadoa Unit (Araújo, 1995), comprises a relatively monotonous, sometimes banded, sequence of allochthonous felsic metatuffs (with porphyritic relic textures) and metatuffites (with variable granulometry and porphyroclastic relic textures). The lower allochthonous unit, labelled Mina do Pequito Unit (Araújo, 1995), is mainly composed by variably metasomatised amphibolites and carbonate and calc-schist rocks that are believed to represent products of the extreme alteration experienced by amphibolites along particular structural settings adjoining the major thrust zone (see below).

In the surrounding region of the Azenhas area, the superimposed effects of the two main Variscan deformation phases (D_1 and D_2) can be recognised (Ribeiro *et al*., 1990; Quesada, 1992; Quesada *et al*. 1994; Araújo, 1995; Araújo and Ribeiro, 1995; Fonseca, 1995). The preserved D_1 thrusts show mylonitic foliations (Fig. 2A) with stretching lineations striking NNE-SSW (Fig. 2B) that display frequent kinematic criteria

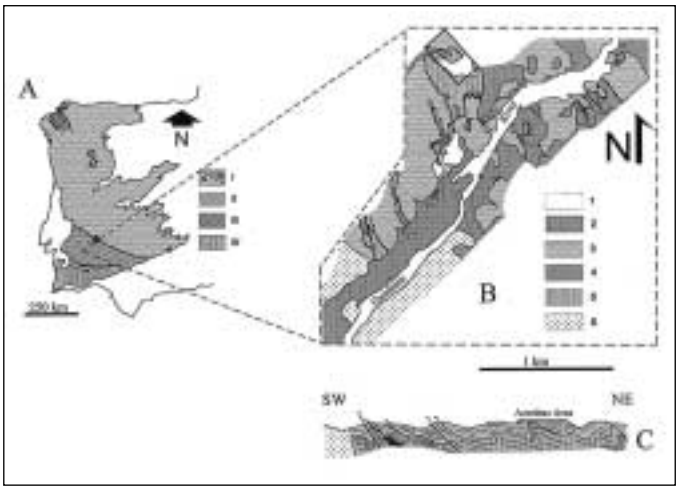

Fig. 1. A: Variscan Terranes in Iberian Peninsula: I. Iberian Autochthonous Terrane (a. sensu stricto, b. Ossa-Morena proximal terrane); II. Oceanic Exotic Terranes; III. Northwest Iberia Polymetamorphic Terranes; IV. South Portuguese Terrane (adapted from Quesada, 1992); B. Geological setting of the Azenhas sector (adapted from Araújo, 1995). 1. Mine tailings; 2. Alluvial deposits; 3. Felsic metavolcanics (Azenha da Rabadoa Unit); 4. Carbonate and calc-schist rocks (Mina do Pequito Unit); 5. Amphibolites (Mina do Pequito Unit); 6. Pedrógão granite. The rectangle corresponds to the area represented in figure 3

Fig. 1. A: Terrenos Variscos de la Península Ibérica: I. Terreno Autóctono Ibérico (a. sensu stricto, b. Terreno proximal Ossa-Morena); II. Terrenos Oceánicos Exóticos; III. Terrenos polimetamórficos del NO Ibérico; IV. Terreno Surportugués (adaptado de Quesada, 1992); B. Esquema geológico del sector da Azenhas (adaptado de Araújo, 1995). 1. Escombreras de mina; 2. Depósitos aluviales; 3. Metavulcanitas ácidas (Unidad Azenha da Rabadoa); 4. Carbonatos y calcoesquistos (Unidad Mina do Pequito); 5. Anfibolitas (Unidad Mina do Pequito); 6. Granito de Pedrógão. El rectángulo corresponde al área representada en la figura 3

(σ-type asymmetric tails and c-s structures), indicating a general movement sense of the hanging wall towards the N. Late mesoscopic D_1 folds with sub-horizontal axes trending E-W are also common (Fig. 2C). According to field data, two major D_2 events can be identified. The first one, D_{2a}, leads to the development of both west-vergent recumbent folds with axes striking N-S to NNW-SSE (Fig. 2D) and top-to-the NNW thrusting. The recognition of en-échelon fold patterns, preservation of several shear criteria at meso- and micro-scale, and orientation of stretching lineations (oblique or sometimes near parallel to the fold axes-Fig. 2E), strongly suggest a sinistral wrench-shear component of deformation (Araújo, 1995; Araújo and Ribeiro, 1995). During the second event, D_{2b}, antiformal stacks developed and the fold axes rotate anticlockwise towards NW-SE direction (Fig. 2D); D_{2b} develops a crenulation cleavage that tends to be steeper, dipping towards NE; the stretching lineations rotate towards ENE-WSW or NE-SW and also plunge to the NE (Fig. 2E). These lineations, are closer to perpendicularity to the major structures, recording the decrease of the sinistral wrench-shear component of deformation during the last pulses of D_2, as comprehensively discussed by Araújo (1995).

Data of Azenhas area

Structural data

In the Azenhas area (Fig. 3), the tectonic contact between the Azenha da Rabadoa and Mina do Pequito Units has been thoroughly examined due to excellent outcrop conditions (photo 1). It forms a relatively narrow and wavy zone of poly-phase thrust movement striking WNW-ESE and dipping less than 45º towards N or NE. Widespread cataclasis related to the late reactivation of this structure in brittle conditions often obliterates the earlier kinematic markers. However, occasional C-S structures coeval of the early movement episodes along this thrust zone can still be locally recognised and indicate predominant thrust movement towards W-SW, although local shear criteria with N-NW transport are preserved. In general, the relative macroscopic homogeneity presented by the hanging wall of the over-thrust block is somewhat disturbed in domains adjoining the main thrust zone, where a 30º, N5ºE stretching lineation in a N60ºW, 30ºNE foliation plane appears, together with some mineralogical and textural transformations (see below).

The footwall amphibolites are, on the contrary, mineralogically and texturally very heterogeneous and are affected by earlier thrusts that are cut by the main thrust zone. The earlier thrusts bring to contact amphibolites with distinct degrees of metasomatism. However, it remains to demonstrate whether the macroscopically similar altered domains correspond to lateral equivalents of each other or not. Amphibolites subjected to pronounced metasomatism are distinctly carbonatised and enriched in magnetite, hosting the once explored small and irregular magnetite ore-bodies whose hanging walls are segments of the major thrust zone or coincide with subsidiary thrust structures.

Within the amphibolite unit, numerous WNW-ESE thrusts dipping, on average, 35ºN and with prevailing thrust shear criteria towards W-SW, cut earlier sub-parallel structures with variable S-SE or NE plunge (usually <45º) occasionally showing northwards movement criteria. Locally, some of these earlier thrusts intersect sub-vertical fractured and hydrothermally altered narrow bands comprising significant

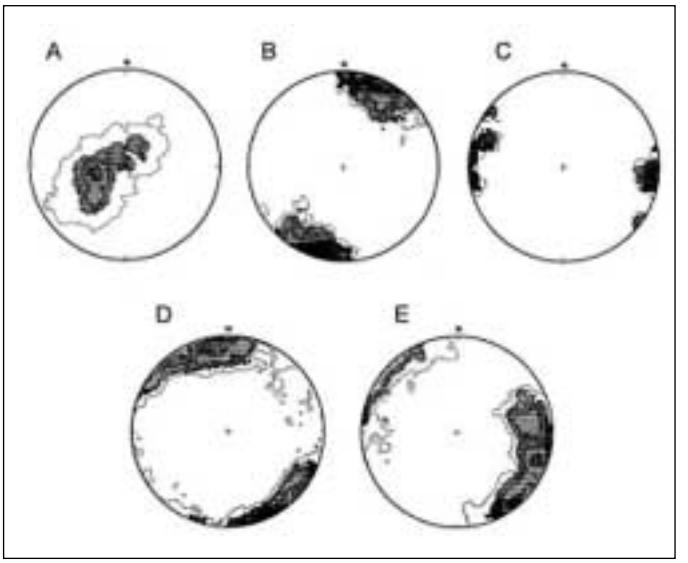

Fig. 2. Equal-area lower hemisphere projection of: A. Foliation (n = 1207; maximum density -N15ºW, 25ºE; contour lines >1; >3; >5; >7%); B. D_1 stretching lineations (n = 218; max. density -5º, N19ºE; contour lines >3; >5; >10; >25%); C. Intersection lineations and D_1 fold axes (n = 36; maximum density -6º, S80ºE; contour lines >10; >15; >25%); D. Intersection lineations and D_2 fold axes (n = 513; maximum density -6º, N10ºW; contour lines >2; >4; >6; >9%); E. D_2 stretching lineations (n = 812; maximum density -6º, S40ºE; contour lines >2; >4; >7; >12%). In last two diagrams the dispersion of orientations is the effect of non-coaxial deformation between D_{2a} and D_{2b}. In fact, in diagram D, the N-S orientations correspond to D_{2a} intersection lineations and fold axes. Later D_{2b} structures present NW-SE orientations. In diagram E, the earlier stretching lineations (D_{2a}) range from NNW-SSE to E-W. Stretching lineations dipping towards ENE correspond mainly to D_{2b}

Fig. 2. Proyección equiareal (hemisferio inferior) de: A. Foliation (n = 1207; densidad máxima -N15ºW, 25ºE; contorno >1; >3; >5; >7%); B. Lineación de estiramiento D_1 (n = 218; densidad máxima -5º, N19ºE; contornos >3; >5; >10; >25%); C. Lineación de intersección y ejes de pliegues D_1 (n = 36; densidad máxima -6º, S80ºE; contornos >10; >15; >25%); D. Lineación de intersección y ejes de pliegues D_2 (n = 513; densidad máxima -6º, N10ºW; contornos >2; >4; >6; >9%); E. Lineación de estiramiento D_2 (n = 812; densidad máxima -6º, S40ºE; contornos >2; >4; >7; >12%). La dispersión de orientaciones en los diagramas D y E es el resultado de la deformación no-coaxial entre D_{2a} y D_{2b}. En D, las orientaciones N-S corresponden a lineaciones de estiramiento, lineaciones de intersección y ejes de pliegues D_{2a}. Las estructuras posteriores D_{2b} muestran orientaciones NW-SE. En el diagrama E, las primeras lineaciones (D_{2a}) varían entre NNW-SSE y E-W. Las lineaciones de estiramiento que buzan hacia el ENE corresponden principalmente a D_{2b}

sulphide dissemination (pyrite ± pyrrhotite ± chalcopyrite).

Locally, sub-vertical (>75º) WNW-ESE left-lateral shears associated to irregular metasomatic bands (commonly enriched in dolomite ± magnetite) cut the early thrusts recognised in the amphibolite unit. Scarce, sub-vertical N70-80E fractures were also identified, often filled by the same mineral assemblage that represents the final metasomatic alteration of the amphibolites. Again, it is worth noting that these relatively late structures never cross the major thrust that brings to contact the Azenha da Rabadoa and the Mina do Pequito Units. As a matter of fact, only the very late NE-SW sub-vertical strike-slip fault zones affect indiscriminately all the rock units and previous thrusts; the major surfaces related to these fault zones preserve slikensides that enable to infer a predominant left-lateral movement.

Petrography and mineral chemistry data

Felsic metavolcanic rocks

Metatuffs of the Azenha da Rabadoa Unit are deformed and mainly composed by quartz, albite and K-feldspar. Accessory amounts of phengite, zircon, green hornblende and ilmenite can also be found, as well as occasional grains of epidote, allanite, calcite and chlorite. Table I lists the average chemical compositions of mineral species for which a representative number of microprobe analyses are available.

Incipient compositional layering may be identified in some of the examined metatuff specimens, particularly in those relatively enriched in green hornblende occurring along the major thrust zone. Primary quartz grains always show optical effects ascribable to heterogeneous work-hardening, probably followed by significant dynamic recovery. This allows quartz to accommodate a significant part of the observed

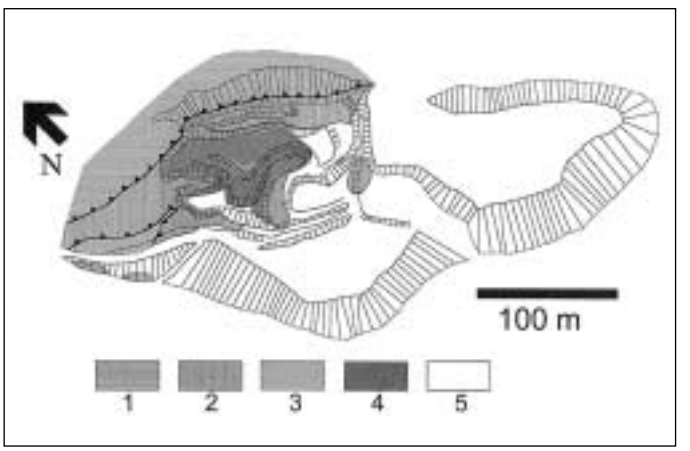

Fig. 3. Schematic geological map of the Azenhas open pit: 1. felsic metavolcanics; 2. amphibolites; 3. calc-schist rocks; 4. dolomitic carbonates; 5. mining dumps. Note that the pit bottom is essentially flat

Fig. 3. Mapa geológico esquemático de la mina a cielo abierto de Azenhas: 1. Metavulcanitas ácidas; 2. Anfibolitas; 3. Calcoesquistos; 4. Carbonatos dolomíticos; 5. Escombreras. A tener en cuenta que el fondo de la corta es esencialmente plano

Average chemical compositions of some mineral species found in metatuffs		
	N	
K-feldspar [(a)]	22	$88.3 \leq Or \leq 90.1$; $8.8 \leq Ab \leq 10.8$
Albite [(a)]	18	$98.4 \leq Ab \leq 99.6$; $0.3 \leq An \leq 1.3$
Hornblende [(b)]	14	$(Na_{0.01}K_{0.01})(Ca_{1.89}Na_{0.10})(Mg_{3.05}Fe_{1.68}Al_{0.15}Mn_{0.09}Ti_{0.02})(Si_{7.63}Al_{0.37})O_{22}(OH)_2$
Ilmenite [(c)]	12	$(Fe_{1.84}Mn_{0.14}Mg_{0.01})(Ti_{2.00}V_{0.01})O_6$

Table I. (a). Mole % of orthoclase (Or), albite (Ab) and anorthite (An) molecules calculated after determination of the cation distribution per formula unit on a basis of 32 oxygens. Cation distributions per formula unit calculated on a basis of (b) 13-(K, Na, Ca) cations and (c) 4 cations, assuming $Fe_t = Fe^{2+}$. In the second column of this and the following tables, N reports the total number of analyses performed for each mineral species

Tabla I. (a) % molar de moléculas de ortoclasa (Or), albita (Ab) y anortita (An) calculada a partir de la determinación de la distribución de cationes por fórmula unitaria calculada sobre la base de (b) 13 cationes (K, Na, Ca) y (c) 4 cationes asumiendo $Fe_t = Fe^{2+}$. En la segunda columna de esta tabla y las siguientes, N representa el número total de análisis realizados para cada especie mineral

deformation and results in a fabric sub-parallel to the macroscopic foliation identified immediately above the major thrust zone. Feldspar deformation by intragranular fracturing is common and increases towards the major thrust zone; mechanical twinning is rare, both in albite and K-feldspar. The brittle deformation of these two silicates favours their subsequent hydrothermal replacement. Therefore, strongly deformed rock domains are mainly composed of secondary minerals resulting from the breakdown of K-feldspar and albite together with primary quartz and fine grained dolomite aggregates that usually fill sub-vertical late micro-fractures.

Amphibolites

The (retrograded) amphibolites of the Mina do Pequito unit are quite heterogeneous and mainly composed of brownish-green and green hornblende, albite, quartz, tremolite, epidote, magnetite and sphene, dolomite and Mg-chlorite occurring as important accessory mineral phases together with sporadic relics of diopside and Cr-spinel. Disseminated pyrite, pyrrhotite and chalcopyrite also occur, but invariably along later micro-fractures, postdating magnetite formation. Table II lists the average chemical compositions of mineral species for which a representative number of microprobe analyses are available.

In samples characteristic of slightly metasomatised amphibolites, a strongly re-crystallised and quartz enriched protolith can be recognised, often showing porphyroblasts of albite in textural equilibrium with pale-green hornblende crystals. These hornblende crystals may sporadically rim extremely corroded diopside grains, and their fringes are often partially replaced by tremolite, which may also form independent aggregates that grow discordantly to the metamorphic fabric. Epidote, dolomite, chlorite and magnetite are relatively scarce in these samples and the chemical composition of Cr-spinel grains is different from the expected, with a less oxidised and Zn-rich core (Table II, formula (j)). As metasomatism intensity increases, products resulting from primary silicate breakdown become more abundant, and the corroded Cr-spinel grains experience a very complex process of alteration that leads to very heterogeneous chemical compositions. Magnetite is one of the outcomes of the process, as suggested by its textural

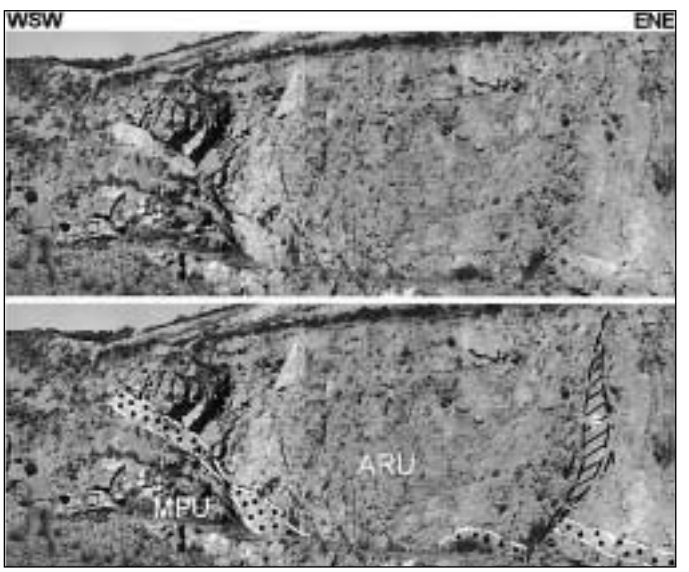

Photo 1. General view of Azenhas open pit: ARU-Azenha da Rabadoa Unit; MPU-Mina do Pequito Unit; F-latter fault; dotted area-thrush zone

Foto 1. Vista general de la costa de Azenhas: ARU: Unidad de Azenha da Rabadoa Unit; MPU: Unidad Mina do Pequito; F: falla tardía; área punteada: zona de cabalgamiento

Average chemical compositions of some mineral species found in amphibolites

	N	
Albite [a]	20	$80.5 \leq Ab \leq 99.3$; $0.4 \leq An \leq 6.2$; $0.4 \leq Or \leq 13.3$
Hornblende [b]	22	$(Na_{0.02}K_{0.02})(Ca_{1.87}Na_{0.12})(Mg_{3.46}Fe_{1.41}Al_{0.08}Mn_{0.03})(Si_{7.67}Al_{0.32})O_{21.98}(OH)_2$ [g]
		$(Na_{0.67}K_{0.07})(Ca_{1.92}Na_{0.01}Mg_{0.07})(Mg_{3.13}Fe_{1.45}Al_{0.31}Mn_{0.05}Ti_{0.02})(Si_{7.1}Al_{0.90})O_{22.01}(OH)_2$ [h]
		$(Na_{0.29}K_{0.01})Ca_{2.00}(Mg_{4.05}Fe_{0.60}Al_{0.29}Mn_{0.05}Ti_{0.01})(Si_{7.54}Al_{0.46})O_{21.99}(OH)_2$ [i]
Diopside [c]	9	$(Na_{0.05}Ca_{0.94})(Mg_{0.72}Fe_{0.24}Al_{0.04}Mn_{0.01})Si_{1.99}O_{6.01}$
Spinels [d]	17	$(Fe^{2+}_{3.09}Mg_{1.53}Mn_{1.15}Zn_{2.28})(Fe^{3+}_{4.02}Cr_{5.29}Al_{6.49}V_{0.08}Ti_{0.06})O_{32}$ [j]
	12	$(Fe^{2+}_{7.39}Mg_{0.12}Mn_{0.50}Zn_{0.01})(Fe^{3+}_{17.17}Cr_{0.06}Al_{0.18}V_{0.08}Ti_{0.50})O_{32}$ [k]
	10	$(Fe^{2+}_{6.16}Mg_{1.96}Mn_{0.07}Zn_{0.03})(Fe^{3+}_{13.19}Cr_{0.02}Al_{2.53}V_{0.05}Ti_{0.05})O_{32}$ [l]
	14	$(Fe^{2+}_{1.94}Mg_{3.45}Mn_{0.42}Zn_{2.20})(Fe^{3+}_{0.51}Cr_{0.04}Al_{15.43}V_{0.01})O_{32}$ [m]
	30	$(Fe^{2+}_{7.86}Mg_{0.11}Mn_{0.02}Zn_{0.01})(Fe^{3+}_{15.95}Ti_{0.03})O_{32}$ [n]
Epidote [e]	13	$Ca_{1.99}(Al_{2.18}Fe^{3+}_{0.81})(Si_{2.98}Al_{0.02})O_{12}(OH)$
Chlorite [f]	10	$(Mg_{4.12}Al_{1.28}Fe^{3+}_{0.54}Mn_{0.04})(Si_{2.78}Al_{1.22})O_{10}(OH)_8$ [o]
	14	$(Mg_{2.11}Al_{1.35}Fe^{3+}_{2.50}Mn_{0.02})(Si_{3.19}Al_{0.81})O_{10}(OH)_8$ [p]

Table II. (a) Mole % of albite (Ab) and anorthite (An) molecules calculated after determination of the cation distribution per formula unit on a basis of 32 oxygens. Cation distributions per formula unit calculated on a basis of (b) 13-(K, Na, Ca) cations, (c) 4 cations, (d) 32 oxygens, (e) 12.5 oxygens, and (f) 14 oxygens assuming $Fe_t = Fe^{2+}$ for pyroxene and amphibole and $Fe_t = Fe^{3+}$ for epidote and chlorite. The Fe^{2+} - Fe^{3+} partitioning in spinels was calculated through an iterative process. In the second column, N reports the total number of analyses performed for each mineral species. Hornblende: (g) average composition of grain cores; (h) and (i) representative analyses of crystal core domains in slightly metasomatised amphibolites. Spinels: (j) average composition of Cr-spinel grain cores included in moderately metasomatised amphibolites; (k), (l) and (m) average compositions obtained for spinel grains within strongly metasomatised amphibolites grouped according to their chemical affinity; (n) average composition of magnetite grains. Chlorite: (o) and (p) average composition of chlorites adjacent to tremolite aggregates and magnetite grains, respectively

Tabla II. (a) % molar de moléculas de albita (Ab) y anortita (An) calculado a partir de la determinación de la distribución de cationes por fórmula unitaria soble la base de 32 oxígenos. Distribución de cationes por fórmula unitaria calculada sobre la base de (b) 13-(K, Na, Ca) cationes, (c) 4 cationes, (d) 32 oxígenos, (e) 12.5 oxígenos, y (f) 14 oxígenos asumiendo $Fe_t = Fe^{2+}$ para piroxeno y anfíbol y $Fe_t = Fe^{3+}$ para epidota y clorita. La partición Fe^{2+} - Fe^{3+} en espinelas se calculó siguiendo un proceso iterativo. En la segunda columna N representa el número total de análisis realizados para cada especie mineral. Hornblenda: (g) composición media del núcleo de los granos; (h) e (i) análisis representativos de núcleos de cristales en anfibolitas ligeramente metasomatizadas. Espinelas: (j) composición media de núcleos de granos de Cr-espinela incluidas en anfibolitas moderadamente metasomatizadas; (k), (l) y (m) composiciones medias de granos de espinela en anfibolitas fuertemente metasomatizadas agrupadas de acuerdo con su afinidad química; (n) composición media de granos de magnetita. Clorita: (o) y (p) composiciones medias de cloritas adyacentes a agregados de tremolita y a granos de magnetita, respectivamente

relationships with epidote, chlorite and tremolite/(green) hornblende aggregates.

Carbonate rocks

As shown in Fig. 3, carbonate rocks form a relatively narrow metasomatic band within the central domain of the mapped area and are apparently confined to an important sub-horizontal thrust that underwent polyphase movement. These rocks are chiefly composed of dolomite, although calcite may be abundant in domains subjected to late fracturing and brecciation. But, irrespective of the chemical nature of the carbonate matrix, the relative abundance of silicate (mostly tremolite, green-brownish hornblende, epidote) and oxide (essentially magnetite) relics is worth noting since they can represent the mineral residue of an amphibolitic protolith (for comparison, see the average chemical compositions of these minerals in Table III).

Both the footwall and hanging wall transition from carbonate rocks towards strongly metasomatised amphibolites proceeds gradually, accompanied by a change in the fabric and mineral compositions, which may lead to calc-schists formation. In these less metasomatised rocks, the average chemical composition of magnetite is slightly different from that obtained for magnetite included in carbonate rocks, being somewhat more enriched in Mg, Mn and Al (Table III).

Average chemical compositions of some mineral species found in carbonate and calc-schist rocks

	N	
Hornblende [(a)]	4	$(Na_{0.02}K_{0.01})(Ca_{1.88}Na_{0.11})(Mg_{3.48}Fe_{1.39}Al_{0.06}Mn_{0.06})(Si_{7.59}Al_{0.40})O_{21.99}(OH)_2$
Tremolite [(a)]	6	$Ca_{1.99}(Mg_{4.89}Al_{0.08}Mn_{0.02})Si_{7.99}O_{22.01}(OH)_2$
Diopside [(b)]	3	$Ca_{0.99}(Mg_{0.93}Fe_{0.04}Al_{0.02}Mn_{0.01})Si_{1.99}O_{5.99}$
Magnetite [(c)]	6	$(Fe^{2+}_{6.75}Mg_{0.72}Mn_{0.08})(Fe^{3+}_{15.59}Al_{0.11}Ti_{0.10})O_{32}$ [(e)]
	4	$(Fe^{2+}_{2.01}Mg_{5.03}Mn_{1.14}Zn_{0.06})(Fe^{3+}_{14.94}Al_{0.83}Ti_{0.04})O_{32}$ [(f)]
Serpentine [(d)]	19	$(Mg_{4.65}Al_{0.35}Fe^{3+}_{0.94}Mn_{0.04})(Si_{3.85}Al_{0.15})O_{9.98}(OH)_8$

Table III. Cation distributions per formula unit calculated on a basis of (a) 13-(K, Na, Ca) cations, (b) 4 cations, (c) 32 oxygens, and (d) 10 cations assuming $Fe_t = Fe^{2+}$ for amphibole and pyroxene and $Fe_t = Fe^{3+}$ for the lizardite-amesite solid solution (Wicks and O'Hanley, 1988). The Fe^{2+} - Fe^{3+} partitioning in magnetite was calculated through an iterative process; (e) average chemical composition for magnetite within carbonate rocks; (f) average chemical composition for magnetite in calc-schists

Tabla III. Distribución de cationes por fórmula unitaria calculada sobre la base de (a) 13 cationes (K, Na, Ca), (b) 4 cationes, (c) 32 oxígenos, y (d) 10 cationes, asumiendo $Fe_t = Fe^{2+}$ para anfíbol y piroxeno y $Fe_t = Fe^{3+}$ para la solución sólida lizardita-amesita (Wicks and O'Hanley, 1988). La partición Fe^{2+} - Fe^{3+} en la magnesita se calculó mediante un proceso iterativo; (e) composición química media de la magnetita en rocas carbonatadas; (f) composición química media de la magnesita en calcoesquistos

Pre-existing silicates are usually almost completely replaced by serpentine aggregates whose average chemical composition is listed in Table III.

Magnetite ores

In the Azenhas area, three main types of magnetite ores can be identified. They occur in distinct lithological and structural settings and exhibit particular fabrics. Massive, fine to medium grained ores form usually large masses within metasomatised amphibolites with incipient carbonatisation when it exists. Banded, medium to coarse-grained ores, on the contrary, are invariably associated with rock domains of intense carbonatisation. Brecciated ores occur in restricted sites of the mapped area and are commonly the result of local fragmentation of massive ores in the vicinity of the late, left-lateral, strike-slip faults.

Magnetite prevails in all ore types, displaying a relative homogeneous chemical composition (Table IV). The interstitial domains of massive ore are usually filled with tremolite aggregates, often partially replaced by serpentine masses whose chemistry is intermediate between lizardite and amesite. Locally, these serpentine masses form intergrowths or are incipiently replaced by optically similar aggregates (although significantly enriched in Mg and Fe^{3+}) tentatively classified as carlosturanite. In banded ores, the interstitial spaces are also occupied by altered aggregates of tremolite, although the presence of scarce and extremely corroded diopside and, exceptionally, Mg-chlorite relics within some serpentine ± carlosturanite masses is also worth noting. Late and irregular calcite ± pyrite veinlets, that cut the magnetite bands at right angles, can also be recognised in some samples. In brecciated ores, the interstitial serpentine ± carlosturanite masses largely predominate over the remaining silicates, being locally intersected by micro-fractures of variable direction filled with Mg-chlorite and another phyllosilicate whose chemical composition is consistent with the lizardite-amesite-cronstedtite solid solution (Table IV); the relative chronology of these late silicates is difficult to assess since no unambiguous textural and crosscutting relationships were observed.

Geochemical data

Representative whole-rock chemical analyses obtained for the main rock types outcropping in the Azenhas area are reported in Table V.

Felsic metavolcanic rocks

The unaltered felsic metatuffs (far from the major thrust zone) display high SiO_2 contents, Na_2O abundances greater than those of K_2O, and a $(CaO+Na_2O+K_2O)/Al_2O_3$ ratio below unity. The obtained Fe_2O_3, MgO, TiO_2 and P_2O_5 contents are low, as well as the incompatible element concentrations (see

Average chemical compositions of some mineral species found in magnetite orebodies

	N	
Tremolite [a]	19	$(Ca_{1.94}Na_{0.05})(Mg_{4.71}Fe_{0.16}Al_{0.04}Mn_{0.09})Si_{7.99}O_{21.99}(OH)_2$
Diopside [b]	4	$Ca_{0.99}(Mg_{0.93}Fe_{0.05}Al_{0.02}Mn_{0.02})Si_{2.00}O_{5.99}$
Serpentine [c]	18	$(Mg_{5.47}Al_{0.21}Fe^{3+}_{0.10}Mn_{0.15})(Si_{3.30}Al_{0.70})O_{10.01}(OH)_8$ [g]
	4	$(Mg_{1.91}Al_{0.03}Fe^{3+}_{3.99})(Si_{3.03}Fe^{3+}_{0.94}Al_{0.02})O_{10.00}(OH)_8$ [h]
Chlorite [d]	9	$(Mg_{4.89}Al_{0.86}Fe^{3+}_{0.22}Mn_{0.02})(Si_{3.18}Al_{0.82})O_{10}(OH)_8$
Carlosturanite [e]	16	$(Mg_{19.94}Fe^{3+}_{0.75}Mn_{0.30})[Si_{10.88}Fe^{3+}_{1.12})O_{27.98}(OH)_4](OH)_{30}.H_2O$
Magnetite [f]	10	$(Fe^{2+}_{7.31}Mg_{0.52}Mn_{0.42}\ Zn_{0.03})(Fe^{3+}_{15.72}Al_{0.06}Ti_{0.02})O_{32}$ [i]
	11	$(Fe^{2+}_{7.14}Mg_{0.92}Mn_{0.21}Zn_{0.02})(Fe^{3+}_{15.74}Al_{0.07})O_{32}$ [j]
	16	$(Fe^{2+}_{7.28}Mg_{0.56}Mn_{0.39}Zn_{0.02})(Fe^{3+}_{15.74}Ti_{0.06})O_{32}$ [k]

Table IV. Cation distributions per formula unit calculated on a basis of (a) 13-(K, Na, Ca) cations, (b) 4 cations, (c) 10 cations, (d) 14 oxygens, (e) 33 cations, and (f) 32 oxygens. For the first two cases, $Fe_t = Fe^{2+}$ was assumed. The Fe^{2+} - Fe^{3+} partitioning in magnetite was calculated through an iterative process; in the remaining cases, all iron was taken as Fe^{3+}. The lizardite-amesite solid solution was considered in (g), while (h) admits its extension towards the cronstedtite composition (Wicks and O'Hanley, 1988). The latter silicate, as well as the reported chlorite, fills up late micro-fractures found in brecciated ores. The ideal chemical composition of carlosturanite given by Guggenheim and Eggleton (1988) was considered in the evaluation of the available microprobe analyses for this mineral. Compositions (i), (j) and (k) report the average chemical composition of magnetite within massive, banded and brecciated ores, respectively

Tabla IV. Distribución de cationes por fórmula unitaria calculada sobre la base de (a) 13 cationes (K, Na, Ca), (b) 4 cationes, (c) 10 cationes, (d) 14 oxígenos, (e) 33 cationes, y (f) 32 oxígenos. En (a) y (b) se asumió $Fe_t = Fe^{2+}$; en el resto de los casos Fe^{2+} - Fe^{3+}. La partición Fe^{2+} - Fe^{3+} en magnetita se calculó mediante un proceso iterativo. En (g) se consideró la solución sólida lizardita-amesita mientras que en (h) se admite su extensión hacia la composición de la cronstedtita (Wicks and O'Hanley, 1988). Este último silicato, así como la clorita rellena microfracturas tardías en menas brechificadas. En la evaluación de los análisis por microonda electrónica disponibles de la carlosturanita se tuvo en cuenta la composición química ideal dada para este mineral por Guggenheim and Eggleton (1988). Las composiciones (i), (j) y (k) representan las composiciones químicas medias de las magnetitas asociadas a menas masivas, bandeadas y brechificadas, respectivamente

discussion below and Fig. 7). Therefore, these rocks can be classified as evolved (meta-)rhyolite tuffs.

Mass balance calculations performed on metatuffs according to the procedure proposed by Gresens (1967), reveal that the mineralogical-textural transformations developed in domains close to the major thrust lead to a volume decrease of the order of 21%, as suggested by the immobile behaviour of Al_2O_3, TiO_2, P_2O_5, Th, Ta and Sc (Fig. 4). Significant loss of SiO_2 (≈ -26 wt%) coupled with a relatively small Fe_2O_3 enrichment (≈ +3 wt%) also occurred, besides minor variations for the remaining analysed elements, easily explained by the chemical composition of the secondary mineral assemblages.

Amphibolites

The original geochemical signature of the amphibolites is at present elusive, because of the effects of the complex and poly-phase metasomatism experienced by these rocks. Their present bulk composition reflects quite well their main mineralogical features. As a matter of fact, the Fe_2O_3, MnO, TiO_2, Zn, Cr and V contents record accurately the relative abundance of spinels in the analysed amphibolites, as well as their prevailing chemical composition; Co is possibly attached to this group of elements, being covariant with Zn. Variations in CaO/Al_2O_3, $(CaO+MgO)/Al_2O_3$ and $(CaO+Na_2O+K_2O)/Al_2O_3$ ratios (0,31-3,26, 0,41-10,56, and 0,73-3,30, respectively) document the relative abundance of Mg-Ca silicates ± epidote and of carbonates, the latter also imparting higher Sr/Ba ratios (ranging from 2 to 8). The covariance between $(Fe_2O_3+MnO)/Al_2O_3$ (ranging from 0,17 to 28,8) and CaO/Al_2O_3 or $(CaO+MgO)/Al_2O_3$ may generally be taken as an expression of the intensity of the chemical transformations caused by the metasomatic processes, correlative to a great extent of the magnetite ore genesis.

Carbonate rocks and magnetite ores

The carbonate rocks belonging to the Mina do Pequito Unit (Table V), are characterised by variable

Fe_2O_3 (± TiO_2 ± MnO ± Zn) concentrations and by significant variations in SiO_2, Al_2O_3, MgO and CaO. All these features are directly expressed in the mineralogy of these metasomatic rocks, particularly in the chemical nature of the carbonate matrix and in the relative abundance of both magnetite and Ca-Mg silicate relics. The same is true for the three ore types, especially the brecciated and banded ores (samples 5 and 9 in Table V, respectively) that have chemical compositions reflecting the mineralogical nature of the accessory components that fill the interstitial spaces. The obtained Fe_2O_3, SiO_2 and P_2O_5 contents are, however, within the compositional ranges reported by Carvalho (1971) for other ore-bodies located in the neighbourhood of the Azenhas area; they never reach an index of high quality iron ores. As expected from the chemical composition of the spinels found in these ores, Zn and V contents are covariant with Fe_2O_3 abundances; Co contents must have an identical explanation.

Discussion

In order to accomplish an alternative metallogenic model for the magnetite ore-bodies of Azenhas area,

Representative whole-rock chemical analyses of the main rock types found in the Azenhas area

	Metatuffs		Variably metasomatised amphibolites					Magnetite ores			Carbonate rocks	
Sp. Nº	*4*	*6*	*1*	*7*	*10*	*11*	*13*	*3*	*5*	*9*	*8*	*12A*
SiO_2	73.02	57.79	59.29	37.37	32.57	20.41	46.59	15.03	21.31	16.16	5.68	2.53
Al_2O_3	13.48	16.98	19.21	20.46	11.58	1.84	7.90	3.16	4.38	0.97	1.84	0.46
Fe_2O_3	1.81	5.68	3.22	7.12	11.77	52.36	10.22	62.50	52.70	28.72	6.51	1.78
MnO	0.04	0.09	0.10	0.77	0.41	0.69	0.20	1.42	1.18	0.88	0.48	0.24
MgO	0.79	2.17	1.92	8.02	22.20	13.43	12.04	12.82	14.29	22.86	10.40	3.91
CaO	1.23	2.46	5.86	21.42	9.25	6.00	16.66	1.62	1.60	11.18	36.34	49.33
Na_2O	7.57	5.07	7.74	0.21	0.26	0.06	0.71	0.06	0.09	0.01	0.05	0.05
K_2O	0.04	0.45	0.49	0.05	0.02	0.01	0.35	0.02	0.02	0.02	0.02	0.01
TiO_2	0.58	0.82	0.30	0.89	0.74	0.08	0.28	0.08	0.17	0.02	0.09	0.02
P_2O_5	0.11	0.19	0.04	0.06	0.15	0.04	0.01	0.02	0.04	0.02	0.01	0.01
LOI	1.33	9.30	2.67	4.13	11.55	4.51	4.32	2.06	4.32	19.32	35.89	40.75
Total	100.00	101.00	100.84	100.50	100.50	99.43	99.28	98.79	100.10	100.16	97.31	99.09
Ba	19	333	290	112	19	2	192	3	61	4	22	6
Sr	30	208	867	412	61	16	392	6	11	67	73	104
Y	33	22	20	16	33	<1	17	3	4	3	3	<1
Zr	245	126	252	27	181	3	58	7	8	5	26	5
V	13	56	9	203	80	66	21	107	94	24	17	8
Cu	12	8	7	7	10	3	7	15	20	3	6	11
Pb	22	<5	34	<5	<5	<5	10	<5	<5	<5	<5	11
Zn	64	115	50	508	264	652	187	873	656	425	126	32
Co	10.9	5.8	3.5	24.9	19.2	49.7	11.3	51	54.9	89.4	2.8	2.4
Cr	0.6	50.9	0.5	448	12.8	6	19.7	6.2	6.3	3.6	8.3	2.5
Sc	11.5	24.3	8.9	36.9	14.6	0.5	5.9	1	1.6	0.5	2	0.6
Ta	<0.3	<0.3	1.2	<0.3	<0.3	<0.3	0.5	<0.3	<0.3	<0.3	<0.3	<0.3
Th	3.9	1.6	15.6	0.5	3.8	0.9	1.4	0.4	0.6	0.1	1.1	0.3
Hf	6.8	3.6	8.2	1.1	5.0	0.2	1.5	0.3	0.2	0.2	0.7	0.2
La	6.1	3.3	0.7	24.4	34.1	3.0	17.0	10.1	5.1	4.7	3.3	1.3
Ce	18	16	5	40	62	7	45	17	12	8	7	3
Nd	10	6	2	10	17	2	18	4	3	2	3	1
Sm	2.78	2.06	1.1	1.94	3.68	0.28	3.46	0.58	0.57	0.35	0.74	0.21
Eu	0.58	0.64	0.26	1.85	1.76	0.12	1.17	0.24	0.2	0.17	0.2	0.07
Tb	0.7	0.5	0.4	0.4	0.9	0.1	0.5	0.1	0.1	0.1	0.1	0.1
Yb	3.67	2.26	2.22	1.88	3.67	0.38	1.38	0.45	0.61	0.33	0.41	0.14

Table V. Oxides of major elements in wt%; trace elements in ppm. Samples 4 and 6 represent metatuffs located far from and close to the major thrust zone, respectively. Samples 3, 5 and 9 represent the massive, brecciated and banded magnetite ores

Tabla V. Análisis químicos representativos (roca total) de los principales tipos de rocas presentes en el área de Azenhas. Óxidos de los elementos mayores en %; elementos traza en ppm. Las muestras 4 y 6 representan metatobas localizadas lejos y cerca de la zona de cabalgamiento principal, respectivamente. Las muestras 3, 5 y 9 corresponden a las menas de magnetita masiva, brechificada y bandeada

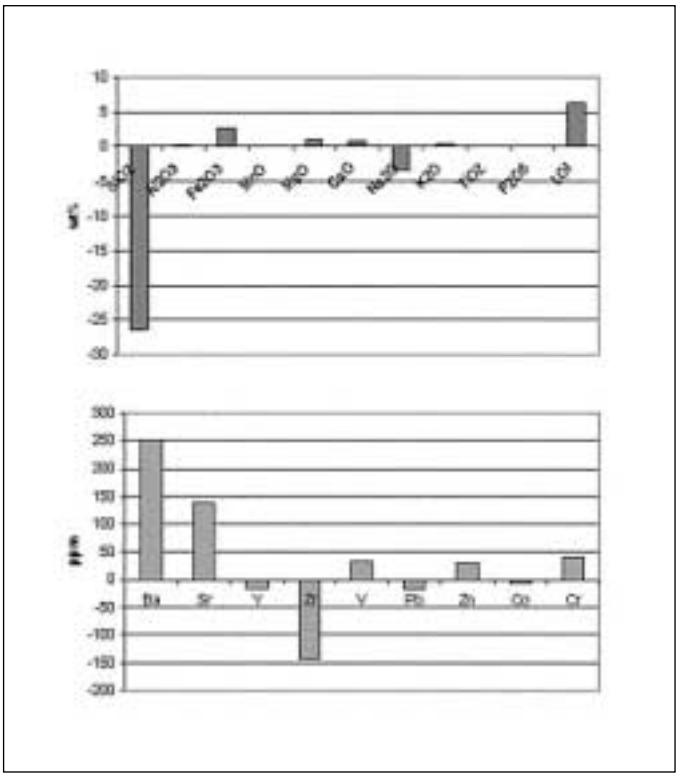

Fig. 4. Main results of mass balance calculation for major and minor elements in felsic metatuffs on the basis of a volume factor of 0.79; the density ratio between samples 4 and 6 is 1.023
Fig. 4. Resultados principales del cálculo de balance de masas para elementos mayores y menores en metatobas ácidas sobre la base de un factor de volumen de 0.79; la relación de densidades entre las muestras 4 y 6 es de 1.023

several issues must be previously discussed, thus supporting the main constraints on the evolution of temperature as a function of the timing of thrusting along a conceptual column that can be used as a reference for quantification purposes.

The available structural data for the Azenhas area provides a strong evidence of a tectonic over-thickening of amphibolites belonging to the Mina do Pequito Unit. The observed geometrical relationships show that the development of the metasomatic processes recorded by the lower domains of the amphibolite sequence took place mainly before the emplacement of the upper slices of amphibolites, therefore preceding the genesis of structures with W-SW thrust shear sense and, consequently, the installation of the felsic metatuffs that are part of the Azenha da Rabadoa Unit.

The local structural pattern is complex, but it is clear from the regional geological mapping and the regional structural data that the thrusts responsible for the thickening of the amphibolite unit should be interpreted as a result of D_1+D_{2a} events, while the major thrust zone that brings to contact the Mina do Pequito e the Azenha da Rabadoa Units corresponds to a D_{2b} feature. Consequently, the development of the earlier thrusts can be envisaged as genetically related to a non-outcropping, D_1 basal thrust zone responsible for the allochthonous emplacement of the entire amphibolite suite. If so, the Mina do Pequito Unit rests tectonically over an autochthonous sequence, presumably the lower levels of the Moura-Ficalho Complex (Middle Cambrian?-Ordovician in age), essentially composed of marbles inter-layered with mafic and felsic metavolcanics (Oliveira *et al*., 1991). This tectonic superposition has never been observed because drilling carried out in the region (300 m of maximum reported borehole depth) around the Azenhas area (Carvalho, 1971) has always stopped within the Mina do Pequito Unit. However, indirect evidence supporting this hypothesis can be obtained from petrographic and geochemical data that suggest an affinity with other allochthonous amphibolite sequences resting over the OMZ autochthon in nearby regions.

Protolith nature and P-T conditions of metamorphism

The very fact that the available data set concerns a particular geological setting where the effects due to late metasomatic processes can dominate largely over pristine characteristics, preclude any accurate tentative to study the metamorphic crystallisation/deformation relationships. Even so, some major constraints can be tentatively articulated, providing a general assessment of some critical parameters necessary for the numerical approach presented below.

Because of the widespread effects due to heterogeneous metasomatism, the chemical nature of the igneous protolith of amphibolites can not be inferred from their major element contents, nor from the relationships established between Ti and trace element (e.g. P, Zr, Nb and Y) abundances, as comprehensively discussed by Rollinson (1993). However, there is no reason to believe that significant variations of Th, Hf and Ta contents have occurred during the metasomatic processes experienced by the amphibolites, and the discriminating diagram proposed by Wood *et al*. (1979) may be used to show that the analysed samples plot within the fields of orogenic and E-MORB basalts. The igneous affiliation thus obtained is, to some extent, distinct from that deduced both for the mafic metavolcanics included in the lower section of the autochthonous Moura-Ficalho Complex (Ribeiro

et al., 1992, 1996), and from the allochthonous amphibolites outcropping in the S. Lourenço and Moinho de Vilares areas (Araújo, 1995), located *ca.* 5 km Southwest of the studied area. The chondrite normalised multi-element diagrams (Fig. 5) do account for the main differences between these three groups of rocks, revealing that: 1) the autochthonous metavolcanics show the most pronounced positive anomalies in Zr, besides slight variations in Y and in Ti; these rocks have thus a chemical signature similar to the one found in continental tholeiites, as referred to by Ribeiro *et al*. (1992, 1996); 2) the geochemical characteristics exhibited by the allochthonous amphibolites of the S. Lourenço and Moinho de Vilares areas are analogous to those commonly recorded by MORB basalts, which, in connection with other kinds of evidence, have been used to interpret these rocks as slices of a strongly dismembered Variscan ophiolite (Araújo, 1995; Fonseca *et al*., 1999); and 3) the amphibolites of Azenhas area, excluding the two strongly carbonatised samples with abundant magnetite, have pronounced negative Ta and Ti anomalies similar to the ones of back-arc basalts, even assuming that part of the relative Ti depletion was achieved during the magnetite ore forming processes. Similar conclusions may be inferred on the basis of the analysis of Zr/Y, Ta/Yb, Th/Yb, $(La/Sm)_{CN}$ and $(La/Yb)_{CN}$ ratios, the latter two taking the chondrite-normalised values for the chemical elements considered. As summarised in Table VI, the values obtained for the amphibolites of Azenhas area deviate clearly from those typically shown by N/T-MORB basalts (e.g. Rollinson, 1993). The ability of many secondary minerals to fix HREE and, sometimes, also Eu, may explain part of that deviation, both suggested by the significant increase of the REE abundances and the distinct chondrite normalised patterns obtained for the strongly carbonatised and magnetite enriched samples (Fig. 6).

From the above data and statements it seems that the igneous protolith of the studied amphibolites is hardly analogous to the parent lithologies of the autochthonous mafic metavolcanics found in the lower section of the Moura-Ficalho Complex, which re-crystallised under P-T conditions of greenschist-amphibolite facies transition (Ribeiro *et al*., 1992, 1996). However, both the Azenhas amphibolites and the S. Lourenço and Moinho de Vilares allochthonous amphibolites may derive from a single root domain if the differences they presently show within their common oceanic signature are explainable by: 1) the geochemical variability of back-arc basalts (Quesada *et al*., 1994; Fonseca *et al*., 1999 and references therein), perhaps enhanced during the metasomatic processes subsequently experienced by the amphibolites of the Azenhas area; or 2) differential crustal contamination during the tectonic imbrication developed after

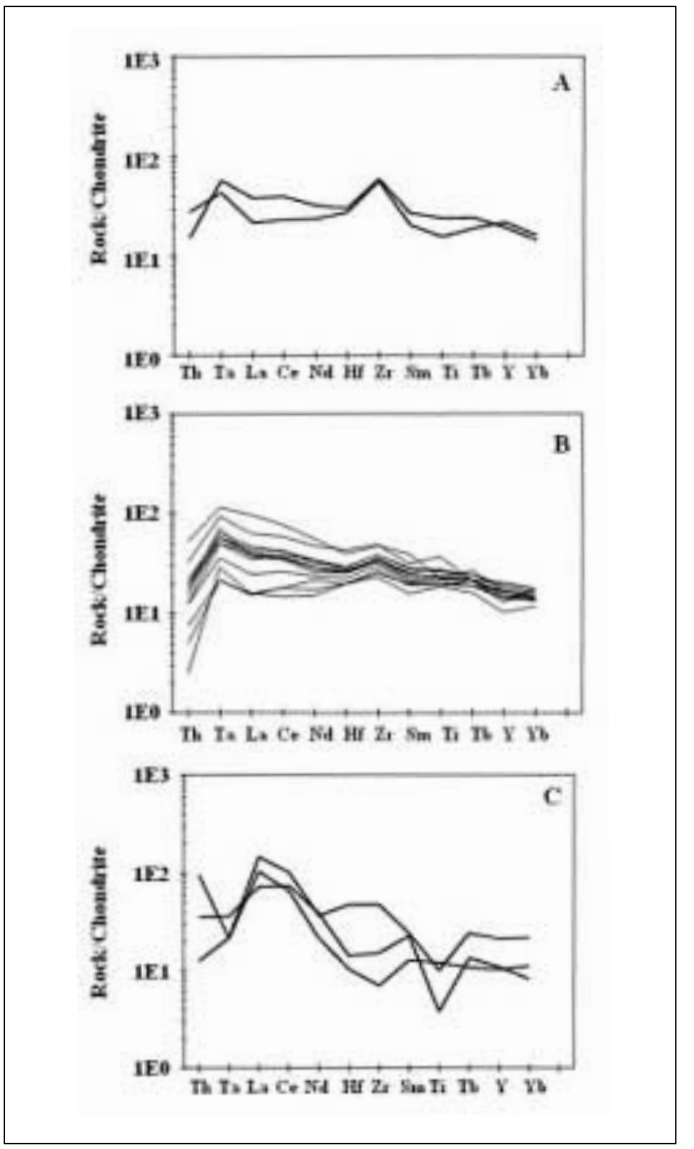

Fig. 5. Chondrite-normalised incompatible element abundance patterns for: A. The autochthonous mafic metavolcanics of the lower section of the Moura-Ficalho Complex; B. The allochthonous amphibolites of the S. Lourenço and Moinho de Vilares areas; and C. the amphibolites of the Azenhas area, excluding the strongly metasomatised samples. A and B plotted using the analytical data reported in Ribeiro *et al.* (1992) and in Araújo (1995), respectively. Chondrite values from Charmichael (1989)

Fig. 5. Diagramas de abundancia de elementos incompatibles (normalizada al condrito) en: A. Metavulcanitas básicas autóctonas de la parte inferior del Complejo Moura-Ficalho; B. Anfibolitas alóctonas de las áreas de S. Lourenço y Moinho de Vilares; y C. Anfibolitas del área de Azenhas, excluyendo las muestras fuertemenre metasomatizadas. A y B a partir de los datos analíticos de Ribeiro et al. *(1992) y Araújo (1995), respectivamente. Los valores condríticos según Charmichael (1989)*

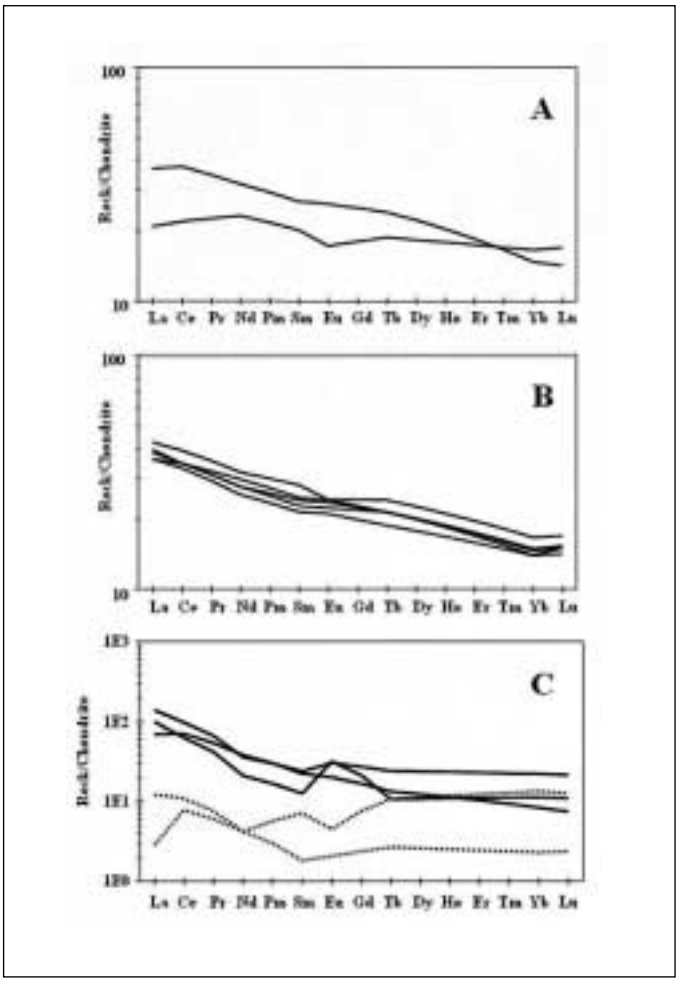

Fig. 6. Chondrite-normalised REE abundance patterns for: A. The autochthonous mafic metavolcanics of the lower section of the Moura-Ficalho Complex; B. The allochthonous amphibolites of the S. Lourenço and Moinho de Vilares areas; and C. The amphibolites of the Azenhas area, including two strongly metasomatised samples (dotted lines). A and B plotted using the analytical data reported in Ribeiro *et al.* (1992) and in Araújo (1995), respectively

Fig. 6. Diagramas de abundancia de REE (normalizada al condrito). A, B y C igual que en la Figura 5

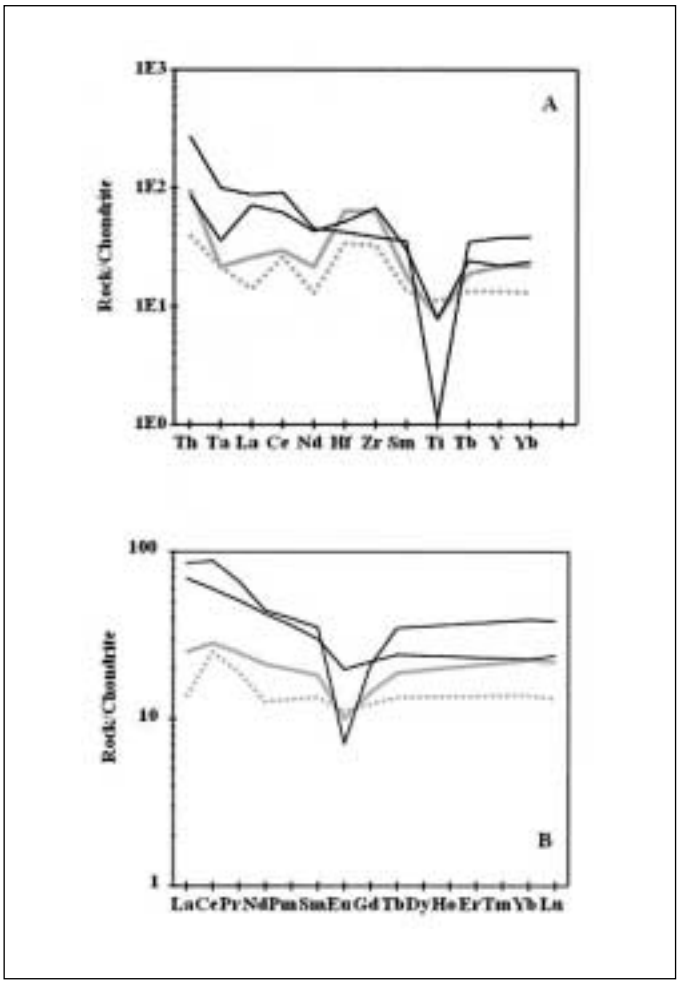

Fig. 7. Chondrite-normalised incompatible element abundance and REE patterns (A and B, respectively) for the autochthonous rhyolite tuffs of the lower section of the Moura-Ficalho Complex (solid thin lines-Ribeiro *et al.*, 1992) and the allochthonous felsic metavolcanics outcropping in the Azenhas area (adjoining and far from the major thrust zone-dotted and solid thick lines, respectively)

Fig. 7. Diagramas de abundancia de elementos incompatibles (A) y REE (B) (normalizada al condrito para las tobas riolíticas autóctonas de la parte inferior del Complejo Moura-Ficalho (líneas finas, Ribeiro et al.*, 1992) y las metavulcanitas ácidas que afloran en el área de Azenhas (cerca y lejos de la zona de cabalgamiento principal: línea de puntos y líneas gruesas, respectivamente)*

obduction (Wilson, 1989). Therefore, according to the available regional data summarised in Fonseca *et al*. (1999), it is thus probable that amphibolites belonging to the Mina do Pequito Unit underwent a P-T-t evolution similar to that recorded by some other allochthonous klippen on top of Palaeozoic sequences within the internal areas of the OMZ. Accepting this inference, the mineralogical features showed by the strong re-crystallised protoliths in slightly metasomatised amphibolites are interpreted as a residue of the (barroisite-)amphibolitic evolving stage. In strong metasomatised amphibolites, the observed carbonatisation is interpreted as caused by degassing processes releasing CO_2 within the over-thrusted autochthonous sequence, the most suitable source for CO_2 being the lower levels of the Moura-Ficalho Complex (Middle Cambrian?-Ordovician in age).

The petrographic and geochemical features (including the mineral chemistry data) displayed by the allochthonous metatuffs of the Azenha da Rabadoa Unit strongly suggests that they have re-

Trace element ratios for allochthonous amphibolites and autochthonous basic metavolcanics					
	Zr/Y	Ta/Yb	Th/Yb	$(La/Sm)_{CN}$	$(La/Yb)_{CN}$
A	1.69 - 5.46	0.30 - 0.54	0.26 - 1.01	0.40 - 6.75	0.84 - 9.35
B	5.29	0.31	0.26	1.40	1.80
C	4.26		0.68	0.92 - 2.21	1.13 - 3.61
D	6.70	0.28	0.32	1.46	2.07

Table VI. A. Amphibolites of the Mina do Pequito Unit, excluding the strongly metasomatised samples. B. Allochthonous amphibolites of the S. Lourenço and Moinho de Vilares areas. C. Allochthonous amphibolites of the upper section of the Beja-Acebuches Ophiolite Complex (BAOC). D. Mafic metavolcanics of the lower section of the Moura-Ficalho Autochthonous Complex. Analytical data for B, C and D extracted from Araújo (1995), Quesada et al. (1994) and Ribeiro *et al.* (1992), respectively. When in presence of significant variable ratios, limits of the obtained ranges are given instead of average values. Unreported Ta contents for BAOC amphibolites prevented the calculation of the respective Ta/Yb ratios

Table VI. Relación de elementos traza en anfibolitas alóctonas y metavulcanitas básicas autóctonas. A. Anfibolitas de la Unidad de Mina do Pequito, excluidas las muestras fuertemente metasomatizadas. B. Anfibolitas alóctonas de las áreas de S. Lourenço y Moinho de Vilares. C. Anfibolitas alóctonas de la parte superior del Complejo Ofiolítico Beja-Acebuches (BAOC). D. Metavulcanitas básicas de la parte inferior del Complejo Autóctono Moura-Ficalho. Los datos analíticos para B, C y D extraidos respectivamente de Araújo (1995), Quesada et al. *(1994) y Ribeiro* et al. *(1992). En casos de alta variabilidad se dan los límites de los valores obtenidos en lugar de los valores medios. La relación Ta/Yb no fue posible en el caso del BAOC al no disponer de datos sobre el Ta*

crystallised under P-T conditions near those of transitional greenschist to amphibolite metamorphic facies. These features are remarkably similar to those found for analogous rocks belonging to the upper part of the autochthonous Moura-Ficalho Complex (Ribeiro *et al*., 1992, 1996). The two diagrams in Fig.7 summarise quite well the strong geochemical affinity of both metavolcanic rock suites, despite the slight differences obtained for the Zr/Y, La/Sm and La/Yb ratios. It is therefore suggested that the root domain of the over-thrust metatuffs is the autochthonous Moura-Ficalho Complex, presently outcropping at *ca.* 15 km East of the Azenhas area.

Dating of deformation events

According to the present state of knowledge it is impossible to judge the individual metamorphic conditions and the relative age of deformation with respect to the metamorphic peak in the Azenhas area. Also unavailable are age constraints such as cooling ages of amphiboles or micas identified in the magnetite ores. Therefore, the limits on the timing of thrusting must be tentatively inferred from regional data that allow constraining the relative dating of the Variscan deformation phases.

The onset of D_1 is somewhat controversial although Early Devonian (*ca.* 395 Ma) represents the most conservative limit, despite the impossibility to discard a very late Silurian age (400-395 Ma)-for comprehensive discussions, see e.g. Araújo, 1995. The geometrical relationships observed between structures ascribed to D_1 and D_{2a} in the autochthonous and allochthonous terranes of OMZ, coupled with several stratigraphic and palaeontology features, strongly suggest that the former event is much older and intense near the suture. As a result, a reasonable estimate for the beginning of D_{2a} is *ca*. 370-385 Ma-see e.g. Araújo, (1995).

Considering the relatively large uncertainties of these time boundaries, only a very rough estimation for the thrust emplacement history at Azenhas area can be performed. It is therefore assumed that the D_{2a} thrusting took place 10 Ma after the D_1 basal thrust zone emplacement and 2 Ma before the development of the late, D_{2b} thrust zones.

Generation of the magnetite ores by thrust induced fluid circulation

All the identified mineralogical and textural transformations in amphibolites record quite well the effects of the early deformation and/or metasomatism experienced by these rocks after thrusting and, presumably, before reaching thermal equilibrium with the autochthonous Moura-Ficalho Complex. Indeed, the precipitation of magnetite in equilibrium with secondary Ca-Mg silicates and the subsequent deposition of dolomite ± serpentine, coupled either with the relative scarcity of Mg-chlorite or with the complex alteration pattern shown by Cr-spinels, are features consistent with the geochemical processes expected to develop in the over-thrusted sequence as the autochthon, much colder, undergoes significant

degassing through prograde metamorphism (Beach and Fyfe, 1972; Fyfe and Kerrich, 1985). This means that the progressive retrograde metamorphism, silica leaching and oxidation, including the magnetite ore genesis, affecting the amphibolites in an early phase, can be largely envisaged as a consequence of the rise of oxidising aqueous fluids under a reversed thermal gradient sustained by the superposition of an allochthonous amphibolitic terrane over an autochthonous greenschist metamorphic sequence.

Subsequent carbonatisation processes, leading to the development of calc-schist and dolomite bands in the vicinity of important thrust segments, indicate that fluid composition became richer in CO_2 with time. The sub-vertical narrow bands of intense fracturing and hydrothermal alteration that comprise both sulphide dissemination (pyrite ± pyrrhotite ± chalcopyrite), and late serpentine ± carlosturanite development, probably record the geochemical effects due to the subsequent superposition of upper amphibolite slices essentially achieved during D_{2a}. The D_{2b} event reinforces the imbricate nature of the whole structure, but, according to the mineralogical record, no long term reverse thermal gradients were established. Indeed, the main evidence of the chemical readjustments induced by the ascent of fluids expelled from the variably metasomatised amphibolites is limited to the notable silica leaching and the slight Fe_2O_3 enrichment displayed by the felsic metatuffs near the major thrust zone. Bearing in mind that the metatuffs are relatively permeable and that no extreme metasomatism is observed in the thrust plane itself (as suggested by mass balance calculations), the amount of fluids out-gassed from the amphibolites during this event was comparably low.

The major intrinsic question on the adequacy of this genetic model concerns therefore the time span needed to generate the magnetite ore-bodies before reaching the thermal re-equilibrium between the early allochthonous amphibolites and the autochthonous sequences of Moura-Ficalho Complex, necessarily established prior to the emplacement of late amphibolite slices and the Azenha da Rabadoa Unit. In this context, it is also critical to understand what is the contribution of the subsequent thrusting event to the overall metasomatic evolution.

Numerical model approach

In order to evaluate the time evolution of the thermal structure of the imbricated rock column, including the time spans of the events under reverse thermal gradients, a one-dimensional numerical model was assembled. Constraints on the timing of thrusting were given before, and the model accounts for the erosion of the thrust column.

The thrust and metasomatic history modelled is summarised in Fig. 8. Over-thrust base temperature is assumed to be 700ºC. The thrust plane is supposed to have been emplaced at around 7 km depth, since this is the estimated thickness of the overlying sediment pile (up to Silurian age) of the autochthonous sequence removed by thrusting. The next thrust emplacement, during D_{2a}, was considered to have occurred 10 Ma later and 1 km above the first thrust. Over-thrust base is assumed to be at 600ºC, according to the mineral paragenesis found in the slightly metasomatised amphibolite slices. The third thrust was placed at about 1 to 1.5 km above the previous one, putting the felsic metatuffs over the heterogeneous amphibolite sequence. The emplacement of D_{2b} thrusts was considered to occur 2 Ma after the second thrusting event, accepting a basal temperature of 500ºC as suggested by the re-crystallisation temperature conditions of metatuffs.

An initial 30 Km thick continental crust is presumed at the beginning of the modelling. Erosion rates were assumed to be equivalent to the present day values in orogenic belts. However, the occurrence of the later thrust events have been fixed according to field data and these may constrain the erosion rate used in model. Several models were run with different types of time dependent erosion rate functions, some of them leading to unrealistic results. The runs presented are just some of the admissible solutions to the model that were found. It must be stressed that the choice of the erosion rate may be critical since it contributes to the advective term of the heat equation and may be an important source of heat dissipation. Both a constant erosion rate equal to present values in mountain ranges and to an erosion rate that linearly decreases with time, were used in the model runs. Every time a thrust occurs, the erosion rate is correspondingly increased, since it also implies some crustal thickening.

The set of rock physical parameters used in the model were obtained from Carmichael (1989) and Turcotte and Schubert (1982), and the list of all model variables is given in Table VII. The initial geotherm was calculated using the equation (Turcotte and Schubert, 1982).

$$T = T_s + \frac{qz}{k} + \frac{\rho H_s h^2}{k}(1 - e^{-z/h})$$

Surface temperature (T_s) was set and kept arbitra-

rily at 0ºC and the heat flux *q* from the base of the crust was fixed so that a geothermal gradient close to 25ºC.Km^{-1} resulted. To compute the thermal evolution of the one-dimensional rock column the heat equation

$$\frac{\partial T}{\partial t} = \kappa \frac{\partial^2 T}{\partial z^2} + U(t)\frac{\partial T}{\partial z} + \frac{A}{pC}$$

was solved numerically. The time dependent erosion rate, $U(t)$, is a function of the type plotted in fig. 9 using run 2 as an example, with the indication of the timings of thrust emplacement. The minimum erosion rate assumed to persist (as a steady state condition) in different runs has been either 0.2 or 0.3 mm.yr^{-1}. Unlike some approaches (Stüwe *et al*., 1993), we assume the onset of erosion at the beginning of the calculations. The boundary condition at the base of the crust uses a thermal perturbation model due to crustal thickening (Stüwe *et al*., 1993), but unlike the approaches made by some authors, it does not consider the entire lithosphere as a way to avoid unrealistic temperatures at the base of the crust (Stüwe *et al*., 1993, 1994; Mancktelow and Grasemann, 1997). The model does not consider any melting in the crust and so it does not allow the temperature of the base of the crust to rise above the granite *solidus* (≈ 820ºC). The evolution with time (t) of the basal crust temperature (T_b) is a sinusoidal function that restores the initial temperature after a given period of time λ (the time span of the thermal anomaly). Its equation is

$$T_b = T_i + \frac{T_{max} - T_i}{2}\left[1 - \cos\left(\frac{2\pi t}{\lambda}\right)\right]$$

The model was run for a maximum time period of 20 Ma, and each run begins with the emplacement of the first thrust. This maximum run time is also the assumed time span for the duration of the thermal anomaly. The value of 20 Ma adopted for λ is not really crucial because all runs have shown that thermal re-equilibration in the upper crust is reached within that time span.

Several runs of the model were performed mainly to assess the influence of different erosion rate time functions; other parameters, such as the time span of the thermal anomaly or even its maximum temperature, do not show any significant differences in the calculated temperatures. Of these, only the runs labelled as 2, 5 and 7 were considered. The different erosion rates adopted in these runs yielded calculated temperatures for the critical events differing by no more than 50ºC, well within the uncertainty of the model and of the data. Significant divergence only occurs in the final moments of the modelling.

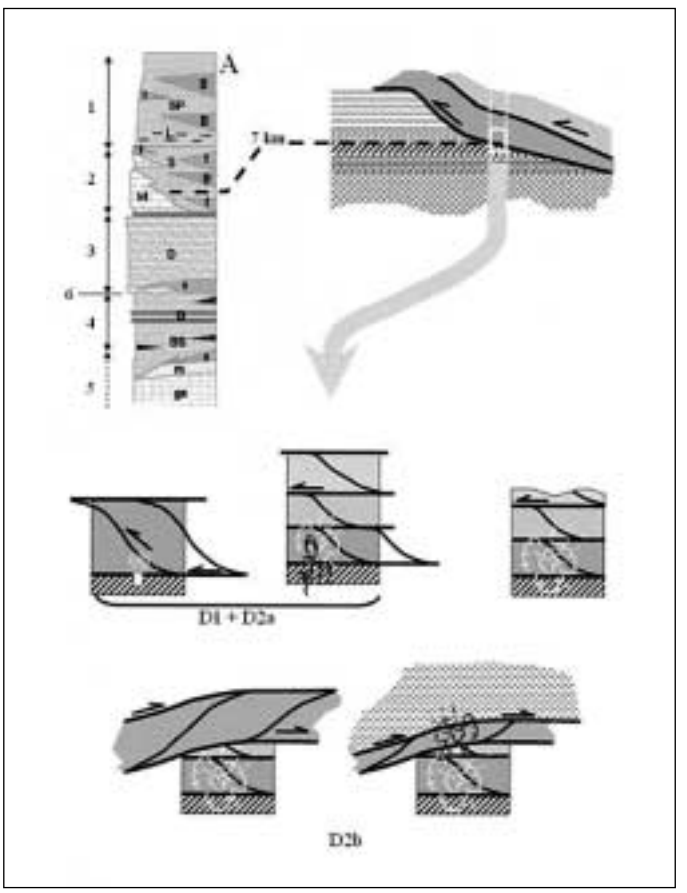

Fig. 8. Schematic representation of the over-thrust sequence evolution at the Azenhas area: A. Stratigraphic sequence of the Montemor-Ficalho autochthonous domain (after Oliveira *et al*., 1991): 1. Xistos de Moura Formation (Ordovician?-Silurian), schists and psamites (SP), lidites (L), mafic (β) and felsic (v pattern) metavolcanics; 2. Moura-Ficalho Volcanic-sedimentary Complex (Middle Cambrian?-Ordovician), calcitic marbles (M), schists (S), mafic (β) and felsic (v) metavolcanics; 3. Dolomitic Formation (Lower Cambrian), dolomites (D, locally silicified), felsic metavolcanics (v) and basal conglomerates; 4. Águas de Peixe Formation, black schists (BS), greywackes (G), black cherts (black); 5. Escoural Formation, micaschists (m), felsic metavolcanics (v), amphibolites and gneisses (ga)

Fig. 8. Representación esquemática de la evolución de la secuencia de cabalgamiento en el área de Azenhas: A. Columna estratigráfica del dominio autóctono Montemor-Ficalho (según Oliveira et al., *1991): 1. Formación Xistos de Moura (Ordovícico?-Silúrico), (SP), esquistos y psamitas, (L) liditas, (β) metavulcanitas básicas, (v) metavulcanitas ácidas; 2. Complejo Vulcanosedimentario Moura-Ficalho (Cámbrico medio?-Ordovícico), (M) mármoles calcíticos, (S) esquistos, (β) metavulcanitas básicas, (v) metavulcanitas ácidas; 3. Formación Dolomítica (Cámbrico inferior), (D) dolomías, localmente silicificadas, (v) metavulcanitas ácidas y conglomerado basal; 4. Formación Águas de Peixe, (BS) esquistos negros, (G) grauvacas, (negro) cherts negros; 5. Formación Escoural, (m) micasquistos, (v) metavulcanitas ácidas, (ga) anfibolitas y gneisses*

Symbols, variables definitions and values used in the numerical model

Symbol	Variable definition	Value	Units
A	Volumetric heat production	1.66×10^{-6}	$W.m^{-3}$
C	Heat Capacity	1000	$J.kg^{-1}.K^{-1}$
h	Characteristic distance	10000	m
H_s	Mass heat production by radioactive decay	6.16×10^{-10}	$W.kg^{-1}$
k	Thermal conductivity	2.4-3.8	$W.m^{-1}.K^{-1}$
q	Conductive heat flux	0.065	$W.m^{-2}$
T	Temperature		ºC
T_b	Temperature at the bottom of the crust		ºC
T_s	Surface temperature	0	ºC
T_i	Initial temperature at the bottom of the crust		ºC
T_{max}	Maximum temperature	820	ºC
t	Time		s
z	Depth		m
$U(t)$	Time dependent erosion rate		$m.s^{-1}$
κ	Thermal diffusivity		$m^2.s^{-1}$
ρ	Density	2700-3100	$kg.m^{-3}$
λ	Duration of thermal anomaly	20	Ma

Table VII. Symbols, variables definitions and values used in the numerical model
Tabla VII. Símbolos, definición de variables y valores usados en el modelo numérico

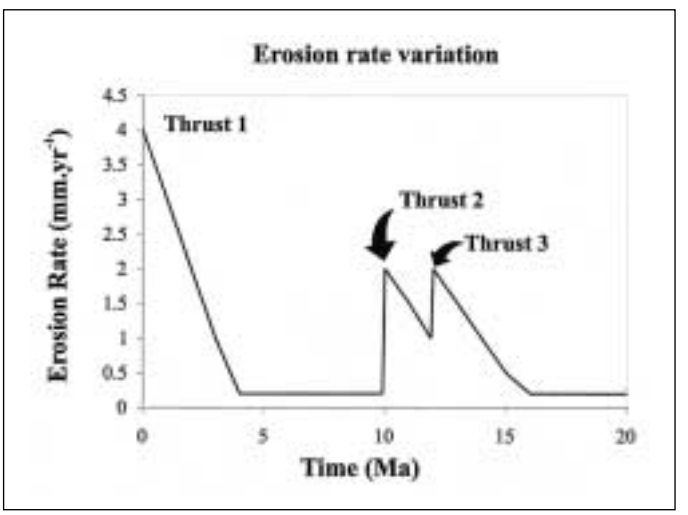

Fig. 9. Erosion rate variation with time. The peaks correspond to each thrust emplacement. This example corresponds to run 2
Fig. 9. Variación temporal de la tasa de erosión. Los picos se corresponden con cada etapa de emplazamiento de los cabalgamientos. Ejemplo correspondiente al intento 2

Model results

The results show that the emplacement of the first thrust is in fact the main event, able to promote significant heat and mass transfer, as can be seen by the continuous rise in the temperature of the underlying rocks for about 5 Ma (Fig. 10). Subsequent thrusting shows that no significant thermal anomaly lasts for enough time to allow important metasomatism in the neighbouring rocks, the anomaly associated to the last thrusting being weak or even absent.

The main differences between the performed runs, whose results are presented in figures 10 to 12, reside in the erosion rates, which are briefly outlined in Table VIII. The obtained results show two important thermal episodes: the first one, after the emplacement of the first thrust, and the second one, during the emplacement of the second and third thrusts. The first episode is clearly the most important because an inverted thermal gradient is kept for over 1 Ma and a regular temperature increase is observed in the underlying rocks lasting for 4.5-5.5 Ma (from a sudden initial increase to 400ºC until a temperature of 500ºC is reached). These conditions are actually very favourable both for the degassing of the hydrated mineral phases of the autochthonous rocks, and for the formation of the magnetite ore-bodies within the over-thrust amphibolites. The second episode is much less pronounced, and also more divergent, although for the window of interest the obtained

results still agree within the uncertainty of the model itself. The reversed thermal gradient appears here in a much smaller scale and dissipates in less than 1 Ma. The increasing temperature of the thrust levels occurs for a period of 2 Ma. This time span seems, however, insufficient to trigger a metasomatic process of an equivalent magnitude of the first one, despite the peak temperature of 530ºC; besides, it affects lithologies whose mineralogical constitution is stable well above that temperature. The emplacement of the third thrust does not cause any significant thermal disturbance unless, like in run 2, the erosion rate is raised, implying a contribution of the advective term to heat transport that causes a temporary increase of the temperature after 12 Ma. This increase in the erosion rate is reasonably assumable only if the late thrust event caused a significant crustal thickening; there is no evidence that this was the case. Nevertheless, this example illustrates well how the advective term may influence the results, showing the need to consider the role of fluid advection in further numerical models.

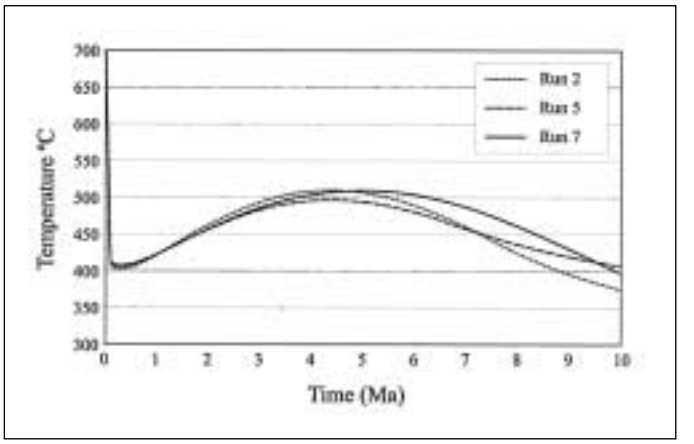

Fig. 10. Temperature variation with time for the allochthonous sequence base after the first thrust emplacement and during the earlier 10 Ma. Parameters for each model reference are given in Table VIII

Fig. 10. Variación temporal de la temperatura en la base de la secuencia alóctona después del primer emplazamiento y durante los 10 Ma siguientes. Los parámetros para cada modelo se dan en la Tabla VIII

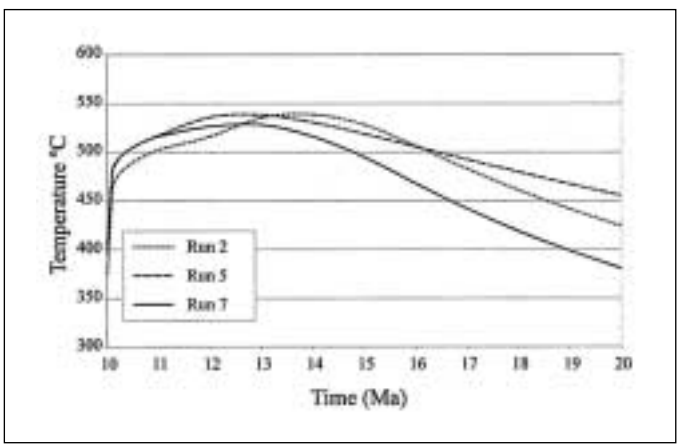

Fig. 11. Temperature variation with time, during the remaining 10 Ma, for the top of the rock sequence immediately below the second thrust plane. Parameters for each model reference are given in Table VIII

Fig. 11. Variación temporal de la temperatura en el techo de la secuencia inmediatamente infrayacente al segundo plano de cabalgamiento durante los 10 Ma subsiguientes a los recogidos en la Figura 10. Los parámetros para cada modelo se dan en Tabla VIII

Conclusions

The imbricated tectonic structure observed at the Azenhas area is the result of poly-phase thrusting achieved during the first two Variscan deformation phases. The tectonic superposition of amphibolites over a relatively cold autochthonous sequence belonging to the Moura-Ficalho Complex (carbonates interlayered with mafic and felsic volcanics) enabled the development of a significant reverse temperature gradient that promoted the rise of oxidising aqueous fluids, subsequently CO_2 enriched. This caused pronounced metasomatism of the over-thrust rocks, leading also to magnetite ore genesis. Later thrusting events reinforced the imbricated structural pattern, and the local geochemical heterogeneity ascribable to the resulting renewed thermal anomalies.

The plausibility of this geological evolution can be put in evidence through several runs of a simple numerical model that accounts both for the thrusting sequence and variable erosion rates. The validity of the developed model in describing a complex geological framework such as the one displayed at Azenhas area may be questioned. But, as shown by Ruppel and Hodges (1994b), results of one-dimensional models do not differ from those obtained by using two-dimensional approaches by more than the intrinsic uncertainty of both kinds of models. Much more critical are: 1) the assumed erosion and exhumation rates; 2) the kind of boundary condition for the base of the crustal section; 3) how fluid circulation is incorporated; 4) the topographic relief (in two-dimensional models); and 5) the attainment, or not, of a steady state solution to the problem (Hanson, 1997 Manning and Ingebritsen, 1999; Ruppel and Hodges, 1994a, 1994b). All these aspects, excluding the topography,

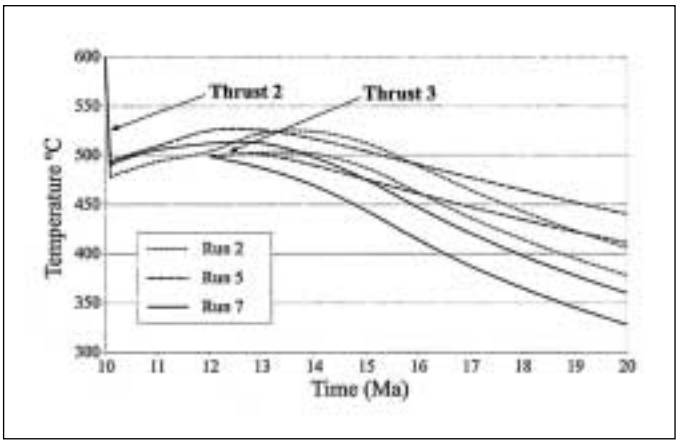

Fig. 12. Temperature variation with time, during the remaining 10 Ma, for the base of the allochthonous sequence formed during the second and the third thrust emplacements. Thrust 3 occurs 1.5 Km above thrust 2. Parameters for each model reference are given in Table VIII

Fig. 12. Variación temporal de la temperatura en la base de la secuencia alóctona formada durante los segundo y tercer eventos de cabalgamiento. El cabalgamiento 3 se sitúa 1.5 Km por encima del cabalgamiento 2. Los parámetros para cada modelo se dan en Tabla VIII

Parameters for the erosion rate for different model runs

Run	U_1 mm.yr^{-1}	U_2 mm.yr^{-1}	U_3 mm.yr^{-1}	U_{min} mm.yr^{-1}	d$U(t)$/dt mm.yr^{-1}.Ma^{-1}
2	4	2	2	0.2	-0.5
5	3.5	2	1	0.2	-0.5
7	3.3	2	1.4	0.3	-0.3

Table VIII. U_i refers to the time dependent erosion rate at the beginning of event i, with $i \in \{1,2,3\}$, which refers to the first, second, and third thrust emplacements respectively. Erosion rate decrease with time is assumed constant and equal for all events. Note that in runs 5 and 7, U_3 is such that no erosion rate increase occurs after the emplacement of the third thrust

Tabla VIII. Parámetros de tasas de erosión aplicados a los diferentes modelos realizados. U_i *se aplica a la tasa de erosión dependiente del tiempo al comienzo del evento* i, *con* $i \in \{1,2,3\}$, *relativo respectivamente al primer, segundo y tercer emplazamiento de cabalgamientos. Se asume que el descenso de la tasa de erosión con el tiempo es constante e igual en los tres eventos. Nótese que en los modelos* 5 *y* 7, U_3 *tiene tales valores que no se produce ningún incremento de la tasa de erosión tras el emplazamiento del tercer cabalgamiento*

can be important to the numerical model here proposed, but their relevance can be diminished with due consideration of the uncertainties involved in the modelling process. Obviously, the accuracy of the results to be obtained cannot be greater than the accuracy of the geological description of the input parameters itself. In this sense, it is unreasonable to seek very detailed modelling at the present state of knowledge. Nevertheless, in the particular case of the model proposed, more than a dozen runs with different input or state parameters, have all resulted in the establishment of a long term thermal anomaly with inverse thermal gradients, thus lending a fair support to our hypothesis for the genesis of the Azenhas magnetite ore-bodies.

The main model results show that the main thrust event developed an inverted thermal gradient for over 1 Ma. More importantly, a regular temperature increase from 400ºC to 500ºC is observed in the underlying rocks for a time interval of 4.5-5.5 Ma. In these conditions the degassing processes of the autochthonous metasediments are promoted, favouring chemical reactions that cause both the breakdown of pre-existent silicates and magnetite precipitation within the over-thrust amphibolites.

For the later thrust episodes the numerical model reveals that the reversed thermal gradient (reaching a peak temperature of 530ºC) has a much smaller scale and dissipates in less than 1 Ma. The increasing temperature of the thrust levels occurs for a period of 2 Ma. In these circumstances, the correlative metasomatism has a lesser magnitude, although supporting the continuing progress of carbonatisation and minor chemical readjustments both in last emplaced amphibolites and in the felsic metatuffs.

Acknowledgements

The authors acknowledge Fundação para a Ciência e Tecnologia through the research grant PBICT/P/CTA/2113/95 - REDIBER and POCTI/3569/1999-MODELIB and the multi-annual grants of the research units CREMINER (Faculdade de Ciências da Universidade de Lisboa) and Centro de Geofísica de Évora (Universidade de Évora). Comments and suggestions by J. Figueiras, Professor José M. Munhá and two anonymous referees were much appreciated.

References

Apalategui, O., Eguiluz. L. y Quesada, C. 1990. Structure. Part V, Ossa-Morena Zone. En: Dallmeyer, R. D. y Martínez Garcia, E. (eds.) Pre-Mesozoic Geology of Iberia. Springer-Verlag, Berlin, 280-291.

Araújo, A. 1995. Estrutura de uma geotransversal entre Brinches e Mourão (Zona de Ossa-Morena): implicações na evolução geodinâmica da margem sudoeste do Terreno Autóctone Ibérico. PhD Thesis, Univ. Évora, Portugal, 200 pg.

Araújo, A. y Ribeiro, A. 1995. Tangential transpressive strain regime in the Évora-Aracena Domain (Ossa Morena Zone). Boletín Geológico y Minero, 106, 111-117.

Beach, A. y Fyfe, W.S. 1972. Fluid transport and shear zones at Scourie, Sutherland: evidence of overthrusting. Contribution to Mineralogy and Petrology, 36, 175-180.

Carmichael, R.S. 1989. Practical handbook of physical properties of rocks and minerals. CRC Press, Boston, 741 pg.

Carvalho, D. 1971. Observações sobre os jazigos de ferro da área Pedrógão-Orada. I Congresso Hispano - Luso - Americano de Geologia Económica, Madrid-Lisboa, 1, 519-537.

Carvalho, D., Goinhas, J., Oliveira, V. y Ribeiro, A. 1971. Observações sobre a geologia do Sul de Portugal e consequências metalogenéticas. Estudos, Notas e Trabalhos do Serviço de Fomento Mineiro, 20, 153-199.

Eguiluz, L., Gil Ibarguchi, J.I., Abalos, B. y Apraiz, A. 2000. Superposed Hercynian and Cadominan orogenic cycles in the Ossa-Morena Zone and related areas of the Iberian Massif. Geological Society of America Bulletin, 112, 1398-1413.

Fonseca, P. 1995. Estudo da Sutura Varisca no SW Ibérico nas Regiões de Serpa-Beja-Torrão e Alvito-Viana do Alentejo. PhD Thesis, Univ. Lisboa, Portugal, 325 pg.

Fonseca, P., Munhá, J., Pedro, J., Rosas, F., Moita, P., Araújo, A. y Leal, N. 1999. Variscan ophiolites and high-pressure metamorphism in southern Iberia. Ofioliti, 24, 259-268.

Fyfe, W.S. y Kerrich, R. 1985. Fluids and thrusting. Chemical Geology, 49, 353-362.

Gresens R.L. 1967. Composition-volume relationships of metasomatism. Chemical Geology 2, 47-65.

Guggenheim, S. y Eggleton, R.A. 1988. Crystal chemistry, classification, and identification of modulated layer silicates. En: Bailey, S.W. (ed.) Hydrous Phyllosilicates (exclusive of micas). Reviews in Mineralogy, Mineralogical Society of America, 19, 675-725.

Hanson, R.B. 1997. Hydrodynamics of regional metamorphism due to continental collision. Economic Geology, 92, 880-891.

Liñan, E. y Quesada, C. 1990. Rift Phase (Cambrian). Part V, Ossa-Morena Zone. En: Dallmeyer R.D. y Martínez Garcia, E. (eds.) Pre-Mesozoic Geology of Iberia. Springer-Verlag, Berlin, 259-266.

Mancktelow, N. y Grasemann, B. 1997. Time-dependent effects of heat advection and topography on cooling histories during erosion. Tectonophysics, 270, 167-195.

Manning, C.E. e Ingebritsen, S.E. 1999. Permeability of the continental crust: implications of geothermal data and metamorphic systems. Reviews of Geophysics, 37, 127-150.

Neiva, J.M.C. 1952. Les mineraux de fer portugais. Estudos, Notas e Trabalhos do Serviço Fomento Mineiro, 7, 281-193.

Oliveira, J.T., Oliveira, V. y Piçarra, J.M. 1991. Traços gerais da evolução tectono-estratigráfica da Zona de Ossa-Morena, em Portugal. Cuadernos Laboratorio Xeologico de Laxe, 16, 221-250.

Quesada, C. 1992. Evolución Tectonica del Maciço Ibérico. En: Gutiérrez-Marco, J.C., Saavedra, J. y Rábano, I. (eds.) Paleozoico Inferior de Ibero-América. Universidad de Extremadura, España, 173-190.

Quesada, C., Apalategui, O., Eguiluz, L., Liñan, E. y Palacios, T. 1990a. Stratigrapphy. Part V, Ossa-Morena Zone. En: Dallmeyer, R.D. y Martínez Garcia, E. (eds.) Pre-Mesozoic Geology of Iberia. Springer-Verlag, Berlin, 252-258.

Quesada, C. y Munhá, J. 1990. Metamorphism. Part V, Ossa-Morena Zone. En: Dallmeyer R. D. y Martínez Garcia, E. (eds.) Pre-Mesozoic Geology of Iberia. Springer-Verlag, Berlin, 314-320.

Quesada, C., Robardet, M. y Gabaldon, V. 1990b. Synorogenic Phase (Upper Devonian - Carboniferous - Lower Permian). Part V, Ossa-Morena Zone. En: Dallmeyer, R.D. y Martínez García, E. (eds.) Pre-Mesozoic Geology of Iberia. Springer-Verlag, Berlin, 273-279.

Quesada, C., Fonseca, P., Munhá, J., Oliveira, J.T. y Ribeiro, A. 1994. The Beja-Acebuches Ophiolite (Southern Iberia Variscan Fold Belt): geological characterisation and geodynamic significance. Boletín Geológico y Minero, 105, 3-49.

Ribeiro, A., Quesada, C. y Dallmeyer, R.D. 1990. Geodynamic evolution of the Iberian Massif. En: Dallmeyer, R.D. y Martínez García, E. (eds.) Pre-Mesozoic Geology of Iberia. Springer-Verlag, Berlin, 398-409.

Ribeiro, M.L., Mata, J. y Piçarra, J.M. 1992. Vulcanismo bimodal da região de Ficalho: características geoquímicas. Comunicações dos Serviços Geológicos de Portugal, 78, 75-85.

Ribeiro, M.L., Munhá J., Mata, J. y Palácios, T. 1996. Vulcanismo na Zona de Ossa-Morena e seu enquadramento geodinâmico. En: Araújo, A. y Pereira, F. (eds.) Estudos sobre a Geologia da Zona de Ossa-Morena-Homenagem ao Prof. Francisco Gonçalves, Évora, 37-56.

Robardet, M. y Gutiérrez Marco, J.C. 1990. Passive Margin Phase (Ordovician-Silurian-Devonian). Part V, Ossa-Morena Zone. En: Dallmeyer, R.D. y Martínez Garcia, E. (eds.) Pre-Mesozoic Geology of Iberia. Springer-Verlag, Berlin, 267-272.

Rollinson, H. 1993. Using geochemical data: evaluation, presentation, interpretation. Longman Group, London, 352 pg.

Ruppel, C. y Hodges, K.V. 1994a. Pressure-temperature-time paths from two dimensional thermal models: prograde, retrograde, and inverted metamorphism. Tectonics, 13, 17-44.

Ruppel, C. y Hodges, K.V. 1994b. Role of horizontal thermal conduction and finite time thrust emplacement in simulation of pressure-temperature-time paths. Earth and Planetary Science Letters, 124, 49-60.

Sánchez Carretero, R., Eguiluz, L., Pascual, E. y Carracedo, M. 1990. Igneous Rocks. Part V, Ossa-Morena Zone. En: Dallmeyer, R.D. y Martínez Garcia, E. (eds.) Pre-Mesozoic Geology of Iberia. Springer-Verlag, Berlin, 292-313.

Silva, J.M. 1945. Gisements de fer du Sud du Portugal. Estudos, Notas e Trabalhos do Serviço de Fomento Mineiro, 4, 31-42.

Stüwe, K., Will, T.M. y Brown, R. 1994. The influence of eroding tipography on steady-state isotherms. Application to fission track analysis. Earth and Planetary Science Letters, 124, 63-74.

Stüwe, K., Will, T.M. y Zhou, S. 1993. On the timing relationship between fluid production and metamorphism in metamorphic piles: some implications for the origin of post-metamorphic gold mineralisation. Earth and Planetary Science Letters, 114, 417-430

Turcotte, D.L. y Schubert, G. 1982. Geodynamics. Application of continuum physics to geological problems. John Wiley & Sons, New York, 450 pg.

Wicks, F.J. y O'Hanley, D.S. 1988. Serpentine minerals: structures and petrology. En: Bailey, S.W. (ed.) Hydrous Phyllosilicates (exclusive of micas). Reviews in Mineralogy, Mineralogical Society of America, 19, 91-168.

Wilson, A. 1989. Igneous petrogenesis. A global tectonic approach. Chapman & Hall, London, 466 pg.

Wood, D.A., Joron, J.L. y Treuil, M. 1979. A re-appraisal of the use of trace elements to classify and discriminate between magma series erupted in different tectonic settings. Earth and Planetary Science Letters, 45, 326-336.

Recibido: julio 2004
Aceptado: febrero 2005